HOW WELL CAN WAVE HEIGHT AND NONLINEAR WAVE STATISTICS BE DETERMINED FROM GRAZING INCIDENCE REMOTE SENSING

BY

CHENGWEI GONG

THESIS

for the degree of

MASTER OF SCIENCE

(Master i Anvendt matematikk og mekanikk)

Department of Mathematics
Faculty of Mathematics and Natural Sciences
University of Oslo

May 2012

Det matematisk- naturvitenskapelig fakultet

University i Oslo

How well can wave height and nonlinear wave statistics be determined from grazing incidence remote sensing

by

Chengwei Gong

Abstract

The motivation of writing this thesis arises in connection with the interpretation of wave measurements: How can the wave height be determined from a grazing incidence radar image? How well can nonlinearity of the ocean surface be distinguished from grazing incidence RADAR images given the fact that the imaging mechanism itself is highly nonlinear? Wave height estimation from RADAR images has traditionally been considered a difficult task. Several fundamentally different approaches have been described for the extraction of wave height. The approach chosen by WAMOS II is based on an empirical formula $\widehat{H_s}(estimated) = A + B\sqrt{SNB}$ proposed for marine RADAR by Nieto Borge(1997,1998) building on established theory for Synthetic Aperture Radar imaging. However, recent theoretical work by Krogstad and Trulsen (2010) suggests that for a nonlinear wave field, the linear dispersion relation may not be revealed by direct Fourier analysis of spatiotemporal data. This may have implications regarding the correct identification of "signal" and "noise" in the signal-to-noise ratio(SNR). In this thesis, numerical simulations of linear and nonlinear wave fields are carried out and used as a basis to generate synthetic radar imaging with grazing incidence. By studying the differences of the remote sensing image-spectra for the linear and nonlinear ocean wave fields, I come to the following conclusion: The signal-to-noise ratio becomes more and more inaccurate as the actual wave height increases. The numerical simulations of nonlinear wave fields are essentially a repetition of recent work by Krogstad & Trulsen.

Acknowledgement

I would like to thank my supervisor Prof. Karsten Trulsen for his great support and guidance. Thank him for his weekly supervision that gradually built up my knowledge and guided me through difficulties, his “paper of hints”, comments on my reports that are very well written and easily understandable, and his tips on how to search a scientific paper online and how to write an official reference. He is very patient in teaching and good at introducing new knowledge to students. I indeed benefit very much from writing this thesis. I would like to thank also my classmate Tore Magnus for helping me with the logarithmic plots.

Contents

Chapter 1

Introduction

1.1 Idea and motivation

There is at present industrial interest in deterministic measurement and prediction of ocean waves. If waves could be measured at some distance, and with sufficient resolution, such that once could achieve advance warning of the occurrence of exceptional or dangerous waves, quiescent periods, or resulting ship motion. With predications: Automated landing of helicopter or airplane on a moving deck, dynamic positioning, more efficient maneuvering, steering of sensitive operations, wider operating windows for marine operations, etc.

The two most feasible remote measurement systems are likely LIDAR and marine RADAR. Both systems can be mounted on ships and platforms, both measure the sea surface with grazing incidence, and they share several challenges regarding interpretation of the measurements. While LIDAR may not work well under certain weather or environmental conditions, marine RADAR suffers from uncertainty about how to interpret the RADAR image.

Marine RADAR was chosen as the designated wave measurement system for the recent industry project "On Board Wave and Motion Estimator" (OWME) coordinated by MARIN, and by the group of Prof. Günther Clauss at the Technical University Berlin. LIDAR was chosen for wave measurements by the group of Prof. Mike Belmont at the University of Exeter. Many other research efforts can be identified around the world. Recently efforts are underway to establish a follow-up OWME-II.

At least two companies offer commercial products capable of extracting directional wave spectra and surface currents from the sea clutter images of marine RADAR, the WAMOS II system of Ocean WaveS, and the two systems WAVEX and "SM-050 Wave and Current Radar" of Miros. And, of significant importance for deterministic wave prediction, it is claimed by Ocean WaveS that the WAMOS II system is capable of extracting single-wave properties of the wave field.

This master thesis will focus on a specific set of problems that arise in connection with the interpretation of wave measurements: How can the wave height be determined from a grazing incidence RADAR image? How well nonlinearity of the ocean surface be distinguished from grazing incidence RADAR images given the fact that the imaging mechanism itself is highly nonlinear?

Wave height estimation from RADAR images has traditionally been considered a difficult task. Several fundamentally different approaches have been described for the extraction of wave height. The approach chosen by WAMOS II is based on an empirical formula

$$H_s = A + B\sqrt{SNR}$$

Proposed for marine RADAR by Nieto Borge (1997, 1998) building on established theory for Synthetic Aperture Radar (SAR) imaging (Alpers and Hassenlmann, 1982). In the above formula H_s is the significant wave height, SNR is the signal-to-noise ratio, and A, B are two empirical parameters that can usually only be determined by a field experimental calibration campaign. Indeed, WAMOS II depends on a field calibration campaign, comparing with e.g. buoy measurements, for reliable estimate of wave height. There are various reasons why the above formula needs an empirical calibration, one being that the Modulation Transfer Function (MTF) for typical marine RADAR is in general not known, SAR should being that it is still not understood why the above formula known to be valid for SAR should also be valid for grazing incidence RADAR.

It has also been proposed to estimate wave height through direct statistical analysis of the radar image. The simplest approach is to estimate the fraction of illuminated surface due to shadowing (Buckley and Aler, 1997; Buckley, 2001). More sophisticated statistical analysis has also been described, e.g. work done by Rune Gangeska attempting analysis of radar image texture for application to Miros RADAR images (Gangeskar, 2000a, b). These methods have apparently not been implemented in practical systems yes.

The Miros wave RADAR does not depend on any calibration campaign for reliable measurements of wave height, and is sometimes quoted as being more reliable for the estimation of wave height than the WAMOS II system. However, the method employed by the Miros wave RADAR is an industry secret not yet published. It should be mentioned here that the Miros wave RADAR is a Doppler RADAR provided by Miros, quite different from the WAMOS II system that allows a variety of standard marine RADAR models to be employed.

Recent theoretical work by Krogstad and Trulsen (2010) suggests that for a nonlinear wave field, the linear dispersion relation may not be revealed by direct Fourier analysis of spatiotemporal data. It is suggested that the phase and group velocities may be different from those expected for wave components below and above the spectral peak. It is also suggested that rather than being a thin dispersion surface, the dispersion relation may be a continuous distribution in Fourier space. This has yet to be verified by experiments, and may affect the

proper interpretation of wave measurements including the interpretation of RADAR images. For example, this may have implications regarding the correct identification of "signal" and "noise" in the signal-to-noise ratio (SNR), and it may affect the correct interpretation of the Doppler shift in order to identify currents.

1.2 Problem description

In this thesis, I carry out numerical simulations of linear and nonlinear wave fields with different design spectra, employing various steepnesses. Two of the nonlinear models described by Krogstad and Trulsen (2010) are employed to account for nonlinearity. These wave fields will be used as a basis for synthesized RADAR imaging with grazing incidence.

We will employ these simulated datasets as a basis for analysis of the simulated radar images. The following types of analysis are included:

Characterize the RADAR image spectrum, and compare with the physical wave spectrum, with particular attention to the distortion of the high frequency tail.

Characterize the observed dispersion relation of the RADAR image, and compare with the observed and theoretical dispersion relations of the physical wave data.

Discuss the feasibility of extracting wave properties directly from the RADAR image, with particular attention to the estimation of wave height.

Study wave field based on the nonlinear Schrödinger equation and its shadowing effect.

This master thesis is essentially an extension of the work of Rune Gangeskar, but starting out from synthetic data rather than field observations. The numerical simulations of nonlinear wave fields are a repetition and extension of the recent work by Krogstad & Trulsen.

1.3 Thesis structure

Chapter 2: 1D linear wave field and its shadowing effect

(Generation of 1D, 1st order ocean waves and computation of their shadow masks)

Chapter 3: 2D linear wave field and its shadowing effect

(Generation of 2D, 1st order ocean waves and computation of their shadow masks)

Chapter 4: Extracting useful wave information from Fourier analysis of the 1D shadow masks

(Generation of 1D, 2nd order nonlinear ocean waves and extraction of wave information from their shadow masks)

Chapter 5: Wave field generated by the nonlinear Schrödinger equation and its shadowing effect

(Solving the NLS equation and extracting wave information from the shadow masks)

Chapter 6: Conclusion

Chapter 2

1D linear wave field and its shadowing effect

2.1 Model for the 1st order ocean surface elevation

In fluid dynamics, wind waves or, more precisely, wind-generated waves that occur on the free surface of oceans are called ocean surface waves. They usually result from the wind blowing over a vast enough stretch of fluid surface. Waves in the ocean can travel thousands of miles before reaching land and range in size from small ripples to huge waves over 30 meters high.

Ocean surface waves have a certain amount of randomness: subsequent waves differ in height, duration and shape, with a limited predictability. They can be described as a stochastic process, in combination with the physics governing their generation, growth, propagation and decay. Therefore, the following mathematical model works reasonably for 1D ocean surface waves.

$$\eta = \sum_j A_j \cos(k_j x - \omega_j t + \phi_j) \quad [1]\ (1)$$

Where η, k, ω, A, ϕ are surface elevation, wave number, wave frequency, wave amplitude and phase shift respectively. The phase shift varies from 0 to2π and is a good description of the stochastic randomness.

In a macro-scopic stand point, surface tension on the ocean surface is not significant comparing to the effect of gravity and thus neglectable. Furthermore, oceans are incredibly deep, for instance, the average depth of the Atlantic Ocean is around 3,926 meters (12,881 feet) and the deepest spot is 8,605 meters (28,232 feet). Due to these two factors, we can well apply the dispersion relation for gravity waves in deep water of infinite depth and the mathematical model immediately becomes:

$$\eta = \sum_j A_j \cos(\frac{\omega_j^2}{g} x - \omega_j t + \phi_j) \quad (2)$$

In conclusion, an ocean surface wave field can be modeled with a group of sinusoidal waves of various frequencies, periods, amplitudes and phase shifts.

2.2 Derivation of the frequency spectrum

In order to find the wave amplitudes in equation (2), we introduce the idea of wave spectrum $S(\omega)$ and its auto-correlation function $R(\tau)$. The spectrum describes the energy distribution of waves among different wave frequencies and is defined as the Fourier transformation of its auto-correlation function. In statistics, the auto-correlation function of a random process describes the correlation between values of the process at different points in time, as a function of the time difference. In signal processing, the above definition is often used without the normalization and defined as:

$$R(\tau) = E[\eta(x,t)\eta(x,t+\tau)]$$

$$= E\left[\left(\sum_j A_j \cos(\, k_j\, x - \omega_j t + \phi_j)\right)\left(\sum_l A_l \cos(\, k_l\, x - \omega_l t - \omega_l \tau + \phi_l)\right)\right]$$

$$= \sum_j \sum_l E\left[A_j A_l \cos\left(k_j x - \omega_j t + \phi_j\right) \cos(k_l x - \omega_l t - \omega_l \tau + \phi_l)\right]$$

$$= \sum_j E\left[A_j^2 \cos\left(k_j x - \omega_j t + \phi_j\right) \cos\left(k_j x - \omega_j t - \omega_j\, \tau + \phi_j\right)\right]$$

$$+ \sum_{j \neq l} E\left[A_j A_l \cos\left(k_j x - \omega_j t + \phi_j\right) \cos(k_l x - \omega_l t - \omega_l \tau + \phi_l)\right]$$

Since ϕ_l is independent of ϕ_j the second part equals to 0, we get:

$$= \sum_{j=1}^{J} \int_0^{2\pi} \left[A_j^2 \cos\left(k_j x - \omega_j t + \phi_j\right) \cos\left(k_j x - \omega_j t - \omega_j\, \tau + \phi_j\right) f(\phi_j)\right] d\phi_j$$

Since $\phi_j$varies from 0 to2π the density function$f\left(\phi_j\right) = \frac{1}{2\pi}$, we get:

$$= \sum_j \int_0^{2\pi} \left[A_j^2 \cos\left(k_j x - \omega_j t + \phi_j\right) \cos\left(k_j x - \omega_j t - \omega_j\, \tau + \phi_j\right) \left(\frac{1}{2\pi}\right)\right] d\phi_j$$

Furthermore, we use the trigonometric formula $\cos(a+b) + \cos(a-b) = 2\cos a \cos b$ and get:

$$= \sum_j \int_0^{2\pi} A_j^2 \left[\frac{\left(\cos(\omega_j \tau) + \cos(k_j x - 2\omega_j t + 2\phi_j - \omega_j \tau)\right)}{2} \left(\frac{1}{2\pi}\right) \right] d\phi_j$$

$$= \sum_j \left(\frac{1}{2\pi}\right) \int_0^{2\pi} \left[\frac{A_j^2}{2} \cos(\omega_j \tau) \right] d\phi_j + \sum_j \left(\frac{1}{2\pi}\right) \int_0^{2\pi} \left[\frac{A_j^2}{2} \cos(k_j x - 2\omega_j t + 2\phi_j - \omega_j \tau) \right] d\phi_j$$

$$= \sum_j \frac{A_j^2}{2} \cos(\omega_j \tau) + \sum_j \left(\frac{1}{2\pi}\right) \frac{A_j^2}{4} \sin[k_j x - 2\omega_j t + 2\phi_j - \omega_j \tau]_0^{2\pi}$$

$$= \sum_j \frac{A_j^2}{2} \cos(\omega_j \tau)$$

Then we determine the two-sided spectrum:

$$S(\omega) = \frac{1}{2\pi} \int_{-\infty}^{\infty} R(\tau)\, e^{-i\omega\tau} d\tau$$

Set the auto-correlation function into the equation:

$$= \frac{1}{2\pi} \int_{-\infty}^{\infty} \sum_j \frac{A_j^2}{2} \cos(\omega_j \tau)\ e^{-i\omega\tau} d\tau$$

Since $\cos(\omega_j \tau) = \frac{1}{2} e^{i(\omega_j \tau)} + \frac{1}{2} e^{-i(\omega_j \tau)}$, we get:

$$= \frac{1}{2\pi} \int_{-\infty}^{\infty} \left(\sum_j \frac{A_j^2}{4} \left(e^{i(\omega_j \tau)} + e^{-i(\omega_j \tau)} \right) \right) e^{-i\omega\tau} d\tau$$

$$= \frac{1}{2\pi} \int_{-\infty}^{\infty} \left(\sum_j \frac{A_j^2}{4} \left(e^{i\tau(\omega_j - \omega)} + e^{-i\tau(\omega_j + \omega)} \right) \right) d\tau$$

$$= \sum_j \frac{A_j^2}{4} \left(\frac{1}{2\pi} \int_{-\infty}^{\infty} e^{i\tau(\omega_j - \omega)} d\tau + \frac{1}{2\pi} \int_{-\infty}^{\infty} e^{-i\tau(\omega_j + \omega)} d\tau \right)$$

Introducing the Kronecker delta function $\frac{1}{2\pi} \int_{-\infty}^{\infty} e^{i\tau(\omega_j \pm \omega)} d\tau = \delta(\omega \mp \omega_j)$, we get the two sided spectrum:

$= \sum_j \frac{A_j^2}{4} \left(\delta(\omega - \omega_j) + \delta(\omega + \omega_j)\right)$	(3)

Applying the normalization rule, we get:

$$\int_{-\infty}^{\infty} S(\omega)\, d\omega = R(0,0)$$

$$\rightarrow \sum_j S(\omega_j)\Delta\omega = \sum_j \frac{1}{2} A_j^2$$

$$\rightarrow S(\omega_j)\Delta\omega = \frac{1}{2} A_j^2$$

$$\rightarrow A_j = \sqrt{2S(\omega_j)\Delta\omega} \quad (4)$$

In conclusion, equation (4) describes wave amplitudes with respect to a given spectral distribution.

2.3 Pierson Moskowitz spectrum

The Pierson-Moskowitz (PM) spectrum is an empirical relationship that defines the distribution of energy with frequency within the ocean. Developed in 1964 the PM spectrum is one of the simplest descriptions for the energy distribution. It assumes that if the wind blows steadily for a long time over a large area, then the waves will eventually reach a point of equilibrium with the wind. This is known as a fully developed sea. To obtain a spectrum of a fully developed sea, Pierson and Moskowitz used measurements of waves made by accelerometers on British weather ships in the North Atlantic. They selected wave data for times when the wind had blown steadily for long times over large areas of the North Atlantic. The following graph is a rough illustration of their experiments.

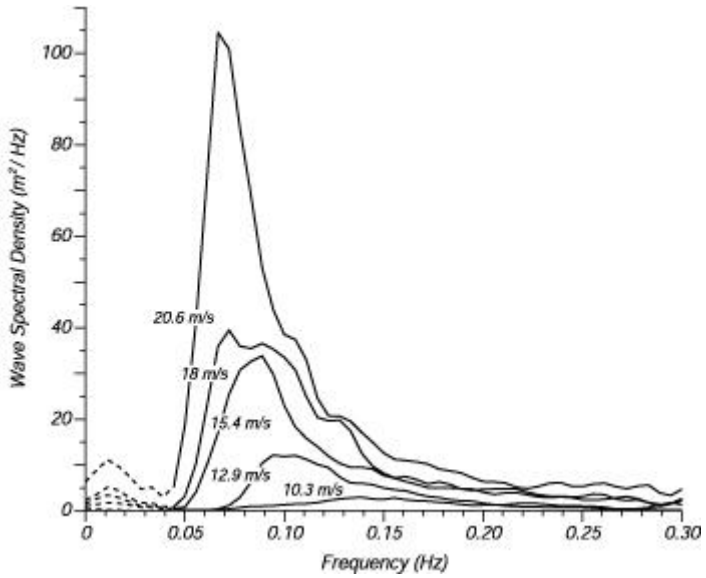

Figure 2.1: Wave spectra of a fully developed sea for different wind speeds according to Moskowitz (1964).

They finally established a mathematical model for the wave spectrum.

$$S(\omega) = \frac{\alpha g^2}{\omega^5} e^{-\beta\left(\frac{g}{\omega U}\right)^4} \qquad [2](5)$$

Where

α is a numerical constant =0.0081

β is a numerical constant =0.74

g is gravity coefficient

U is the wind speed at 19.4m above the sea surface.

From the stand point of doing numerical experiments, it is convenient to set $\omega_p = g/U$ as the peak wave frequency so as to have a control over the dominating wave frequency in the PM spectrum.

2.4 Construction of the ocean surface elevation

After having defined all the variables in equation (2), we may implement the mathematical model with the following Matlab code:

```
function eta1(L,T,M,N,omegaP,filename)
%L-spatial length;
%T-time length;
%M-num. of spatial points;
%N-num. of time points;
%omegaP-peak wave frequency in PM-spectrum
alpha=0.0081;
beta=0.74;
g=9.8;
%Discretize omega.
d_omega=0.2;
omega_max=6;
omega_min=0.2;
omega=omega_min:d_omega:omega_max;
J=(omega_max-omega_min)/d_omega+1;
%Discretize k
k=omega.^2/g;
%Create the spectrum.
S=((alpha*g^2)./omega.^5).*exp(-beta.*(omegaP./omega).^4);
%Construct the coefficients Aj.
A=sqrt(2*S*d_omega);
%Discretize the time.
dt=T/N;
%Discretize the distance.
dx=L/M;
[x,t]=meshgrid(0:dx:L-dx,0:dt:T-dt);
%load phase
structure=load('phase','-mat');
phi=structure.phi;
%Construct the wave elevation.
eta=0;
for j=1:J
    eta_frag=A(j)*cos(omega(j)^2/g*x-omega(j)*t+phi(j));
    eta=eta+eta_frag;
end
x=x(1,:);
t=t(:,1)';
save(filename,'x','t','eta','L','T');
fprintf('Sea surface creation is done.\n');

%Take this out for other uses in other chapters
function phase()
d_omega=0.2;
omega_max=6;
omega_min=0.2;
J=(omega_max-omega_min)/d_omega+1;
for j=1:J
    phi(j)=2*pi*rand(1);
end
save('phase','phi');
```

Figure 2.2 and 2.3 are the synthetic ocean surface waves generated by the codes. The former has a shorter spatial length while the later has a longer one, and they are both at time point $t = 0$.

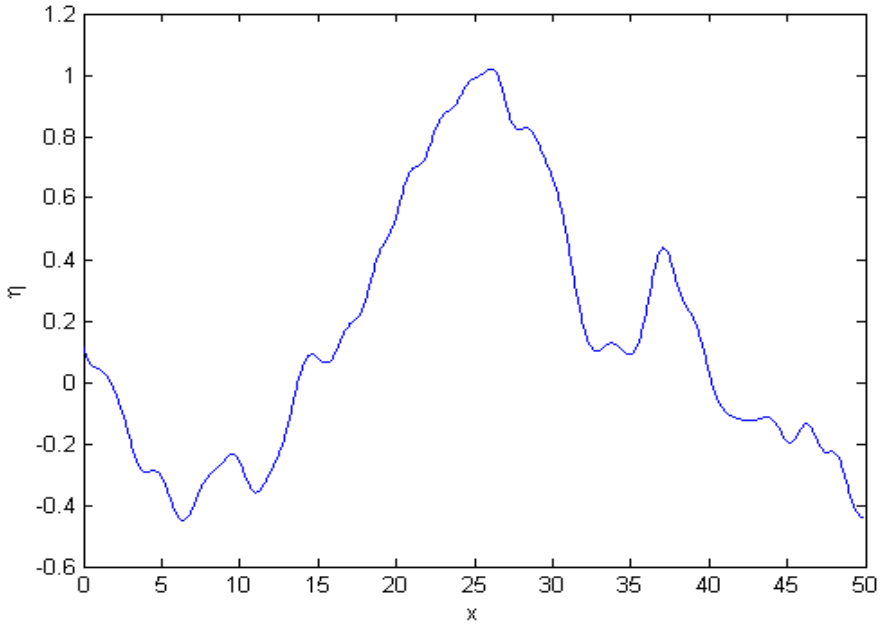

Figure 2.2: 1D ocean surface waves in a short distance

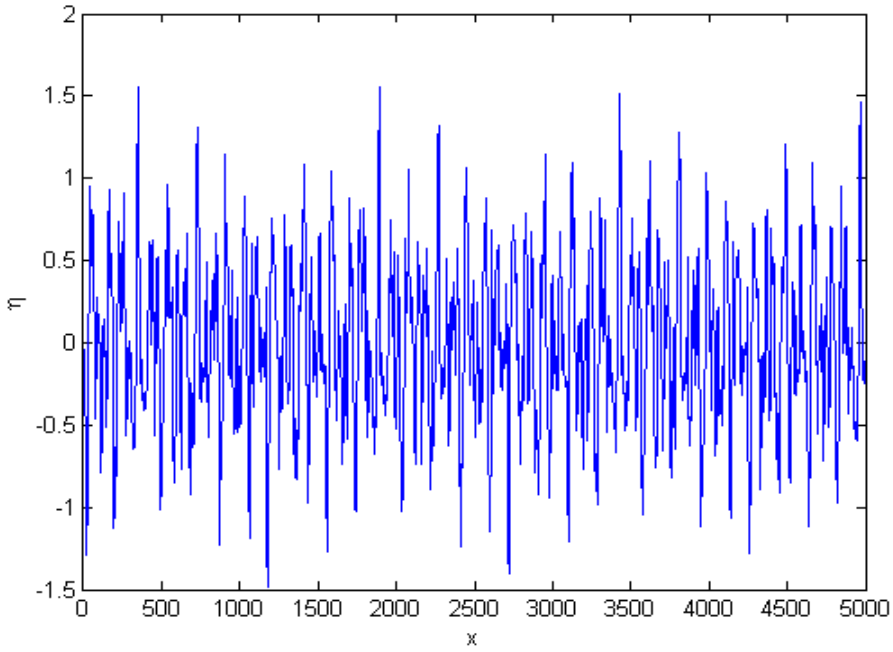

Figure 2.3: 1D ocean surface waves in a long distance

In conclusion, ocean surface waves are modeled as a combination of many monochromatic waves with different properties and they are highly stochastic.

2.5 Computation of the shadow masks

By detecting waves on the ocean surface with a spatially fixed radar, we observe a radar image consisting of visible portions ("islands") of reflection as well as shadowed regions of no reflection ("troughs"). A "shadow mask" is defined by representing "islands" with "1"s and "troughs" with "0"s. It is not possible to give an analytical function for the shadow mask of a surface wave field, consisting of the superposition of many partial waves. Therefore shadow masks are usually found by numerical computations.

We shall first establish a mathematical model to find shadow masks. We assume a given sea surface $\eta(x_n)$ with interpolation points $x_n$on the x-axis and a fixed radar at the point of $(0, h)$ on the xz-plane. First of all, we establish a line-function to represent the path that light reflects from waves to the radar, notice that the line-function goes through two points $(0, h)$ and $(x_n, \eta(x_n))$, so we calculate:

$$l = \frac{\eta_n - h}{x_n} x + h \tag{6}$$

Furthermore, we need to check, for a selected point on the surface η_n, whether the heights of all its previous points: $\eta_{n-1}, \eta_{n-2}, \dots, \eta_1$ exceed the corresponding z-values of the line-function $l_{n-1}, l_{n-2}, \dots, l_1$. That is to check if:

$$\eta_m \geq l_m, \quad where \ m < n \tag{7}$$

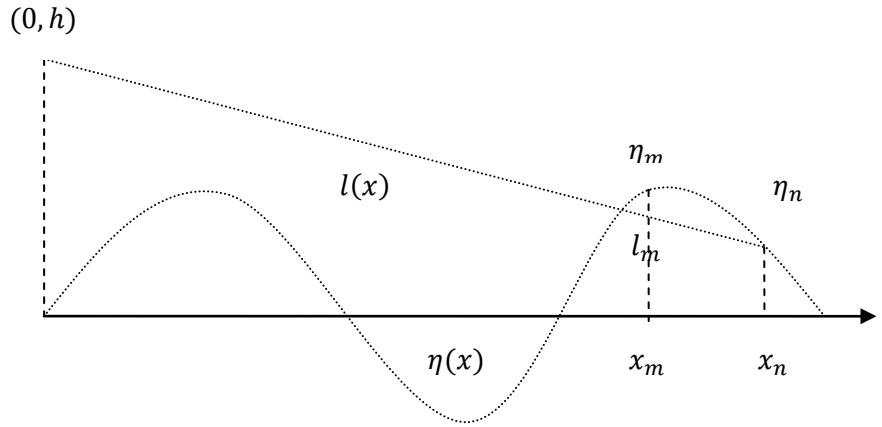

Figure 2.4: 1D shadow mask analysis

From the graph, we could clearly observe that if condition (7) is fulfilled for any given point-η_n, and then η_n is shadowed by a point ahead of it and thus not visible to the radar.

Implement the mathematical model with MATLAB code:

```
s=size(eta);
Sm=ones(s(1),s(2));
%calculate the shadow mask matrix Sm.
for k=1:s(1) %iterator of time
    for i=1:s(2) %iterator of distance
        yl=(eta(k,i)-H)/x(i)*x+H;
        res=yl-eta(k,:);
        cross=find(res<0,1);
        if cross<i
            Sm(k,i)=0;
        end
    end
end
```

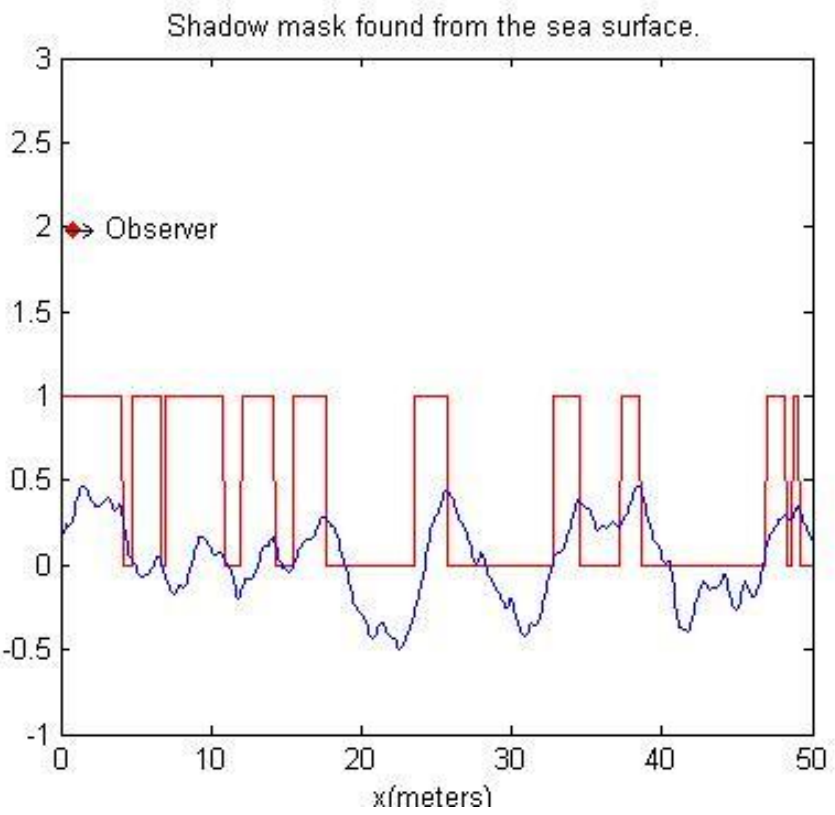

Figure 2.5: 1D shadow mask

For Figure 2.5, radar is set to the marked point (0,2) and the red curve is the shadow mask simulated from the 1D ocean surface. One can easily check the correctness by using a ruler.

2.6 Discrete Fourier transform

In mathematics, the discrete Fourier transform (DFT) is a specific kind of discrete transform, used in Fourier analysis. It transforms one function into another, which is called the frequency domain representation, or simply the DFT, of the original function. The DFT requires an input function that is discrete. Such inputs are often created by sampling a continuous function. The discrete input function must also have a finite duration, such as one period of a periodic sequence. FFT algorithms are so commonly employed to compute DFTs that the term "FFT" is often used to mean "DFT" in colloquial settings. Formally, there is a clear distinction: "DFT" refers to a mathematical transformation or function, regardless of how it is computed, whereas "FFT" refers to a specific family of algorithms for computing DFTs. The terminology is further blurred by the synonym finite Fourier transform for the DFT, which apparently predates the term "fast Fourier transform" [3].

In Matlab, the discrete Fourier transform is implemented as the followings:

$$fft(x_n) = \sum_{n=0}^{N-1} x_n \, e^{-\frac{2\pi i}{N} k_n}$$

$$ifft(X_k) = \frac{1}{N} \sum_{n=0}^{N=1} X_k \, e^{\frac{2\pi i}{N} k_n}$$

We shall use these to find out wave spectra and image spectra of shadow masks in next section.

2.7 Wave and image spectra

As being discussed in the previous sections, surface waves can be constructed by giving the spectrum (frequency or wave number spectrum). On the other way around, we can extract the spectrum by sampling the waves. A general way of doing this is to compute the Fourier transform $\hat{\eta}(k,\omega)$ of $\eta(x,t)$, and the spectrum immediately becomes $\hat{S}(k,\omega) = |\hat{\eta}(k,\omega)|^2$. The difference between $\hat{S}(k,\omega)$ and the PM-frequency spectrum in section 2.3 is that $\hat{S}(k,\omega)$ contains one more variable k- the wave number. Under this circumstance, a contour-plot of $\hat{S}(k,\omega)$ reveals the dispersion relation. Since x and t in equation (2) have opposite signs, fft and $ifft$ have to be applied in turn. The Matlab code for this is:

```
%DFT for the surface elevation.
s=size(eta); %eta(t,x);
N=s(1); %number of columns (num of time levels)
eta_hat=1/N*fft(ifft(eta).').';
eta_hat=fftshift(eta_hat);
eta_estimator=(abs(eta_hat)).^2;
```

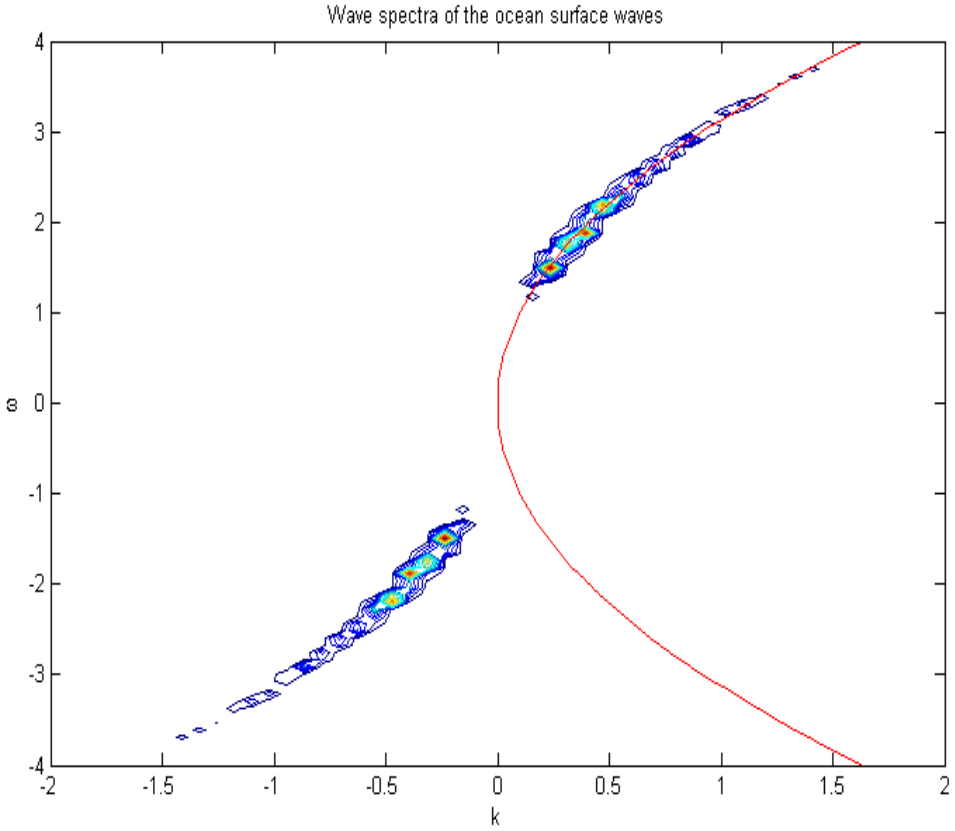

Figure 2.6: wave spectra of 1D ocean surface waves

In figure 2.5, the red, parabolic curve is the function of dispersion shell $k = \frac{\omega^2}{g}$. The contour plot is symmetric around the origin and part of the contour lies along the theoretical dispersion function. This method makes it possible to observe the dispersion relation from surface waves measured.

With the same method, we compute the Fourier transform $\widehat{Sm}(k, \omega)$ of the shadow masks $Sm(x, t)$, and the image spectrum becomes $\hat{I}(k, \omega) = \left|\widehat{Sm}(k, \omega)\right|^2$. Matlab code for this is:

```
%DFT for the shadow mask.
sm_hat=1/N*fft(ifft(sm).').';
sm_hat=fftshift(sm_hat);
sm_estimator=(abs(sm_hat)).^2;
%re-construct omega for plots.
n_omega=0:N-1;
omega2=2*pi*(n_omega-round(N/2))/T;
%re-construct k for plots.
n_k=0:M-1;
k2=2*pi*(n_k-round(M/2))/L;
%create meshgrids for k and omega.
[k,omega]=meshgrid(k2,omega2);
```

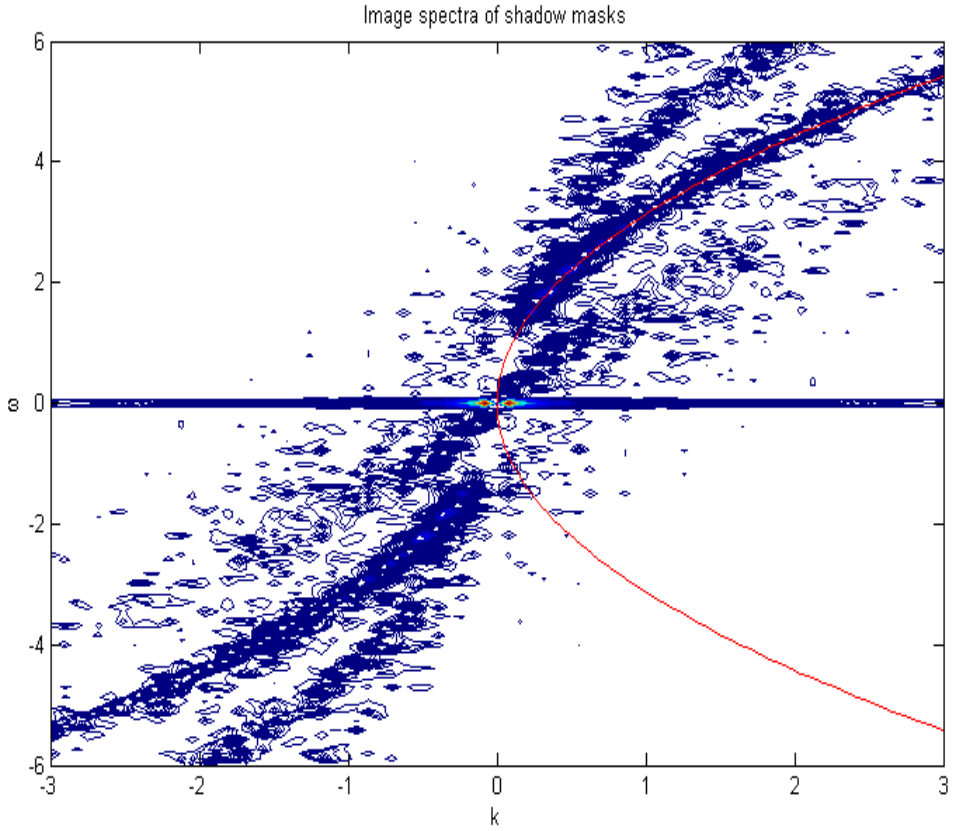

Figure 2.7: Image spectra of 1D shadow masks

In figure 2.6, the contours lie dispersed along different harmonic shells from the lowest reclined –the 0^{th} harmonic to the highest parabolic shaped- the 2^{nd} harmonic. Theoretically speaking, there are infinitely many harmonic shells and they are all partly occupied by these contours. By comparing figure2.6 with figure2.7, we also notice that the image spectra mantle the wave spectra, in other words, the image spectra contain useful information of the waves. By filtering out the useful information from the image spectra, we can estimate many properties of the waves including the significant wave height. We should discuss the topic in next chapters.

Chapter 3

2D linear wave field and its shadowing effect

3.1 Derivation of the auto-correlation function

Similar to the one dimensional case, a monochromatic wave is generated by:

$$A\sin(k_x x + k_y y - \omega t + \phi)$$

A superposition of many monochromatic waves gives rise to the 2D ocean surface:

$$\sum_n \sum_m A_{n,m} \sin(\, k_x(\omega_n, \theta_m)x + k_y(\omega_n, \theta_m)y - \omega_n t + \phi_{n,m})$$

Applying the dispersion relation for gravity waves in infinitely deep water:

$$\omega = \sqrt{gk} = \sqrt{g\sqrt{k_x^2 + k_y^2}}$$

$$k_x = k\cos\theta = \frac{\omega^2}{g}\cos\theta$$

$$k_y = k\sin\theta = \frac{\omega^2}{g}\sin\theta$$

We get:

$$= \sum_n \sum_m A_{n,m} \sin(\frac{\omega_n^2}{g}\cos\theta_m\, x + \frac{\omega_n^2}{g}\sin\theta_m\, y - \omega_n t + \phi_{n,m})$$

To find the amplitude $A_{n,m}$, first of all, we calculate the auto-correlation function:

$$R(\xi, \zeta, \tau) = E[\eta(x, y, t)\eta(x + \xi, y + \zeta, t + \tau)]$$

$$= E\left[\left(\sum_n\sum_m A_{n,m}\sin(k_x x + k_y y - \omega_n t + \phi_{n,m})\right)\left(\sum_p\sum_q A_{p,q}\sin(k_x x + k_y y - \omega_p t + \phi_{p,q} + k_x\xi + k_y\zeta - \omega_p\tau)\right)\right]$$

$$= \sum_n\sum_m E[A_{n,m}^2\sin(k_x x + k_y y - \omega_n t + \phi_{n,m})\sin(k_x x + k_y y - \omega_n t + \phi_{n,m} + k_x\xi + k_y\zeta - \omega_n\tau)]$$

$$+ \sum_{(n,m)}\sum_{\neq(p,q)} E[A_{n,m}A_{p,q}\sin(k_x x + k_y y - \omega_n t + \phi_{n,m})\sin(k_x x + k_y y - \omega_p t + \phi_{p,q} + k_x\xi + k_y\zeta + \omega_p\tau)]$$

Since $\phi_{n,m}$ is independent of $\phi_{p,q}$ the second part equals to0, and we get:

$$= \sum_n\sum_m \int_0^{2\pi}[A_{n,m}^2\sin(k_x x + k_y y - \omega_n t + \phi_{n,m})\sin(k_x x + k_y y - \omega_n t + \phi_{n,m} + k_x\xi + k_y\zeta - \omega_n\tau + \phi_{n,m})f(\phi_{n,m})]d\phi_{n,m}$$

Since $\phi_j$varies from 0 to2π the density function becomes $f(\phi_{n,m}) = \frac{1}{2\pi}$, and we get:

$$= \sum_n\sum_m \int_0^{2\pi}\left[A_{n,m}^2\sin(k_x x + k_y y - \omega_n t + \phi_{n,m})\sin(k_x x + k_y y - \omega_n t + \phi_{n,m} + k_x\xi + k_y\zeta - \omega_n\tau + \phi_{n,m})\left(\frac{1}{2\pi}\right)\right]d\phi_{n,m}$$

By using the trigonometric formula $\cos(a+b) - \cos(a-b) = -2\sin a\sin b$, we get:

$$= \sum_n\sum_m \int_0^{2\pi} A_{n,m}^2\left[\frac{(\cos(k_x\xi + k_y\zeta - \omega_n\tau) + \cos(2k_x x + 2k_y y - 2\omega_n t + 2\phi_{n,m} + k_x\xi + k_y\zeta - \omega_n\tau))}{2}\left(\frac{1}{2\pi}\right)\right]d\phi_{m,n}$$

$$= \sum_n\sum_m\left(\frac{1}{2\pi}\right)\int_0^{2\pi}\left[\frac{A_{n,m}^2}{2}\cos(k_x\xi + k_y\zeta - \omega_n\tau)\right]d\phi_{m,n} + \sum_n\sum_m\left(\frac{1}{2\pi}\right)\int_0^{2\pi}\left[\frac{A_{n,m}^2}{2}\cos(2k_x x + 2k_y y - 2\omega_n t + 2\phi_{n,m} + k_x\xi + k_y\zeta - \omega_n\tau)\right]d\phi_{n,m}$$

$$= \sum_n\sum_m\frac{A_{n,m}^2}{2}\cos(k_x\xi + k_y\zeta - \omega_n\tau) + \sum_n\sum_m\left(\frac{1}{2\pi}\right)\frac{A_{n,m}^2}{4}\sin[2k_x x + 2k_y y - 2\omega_n t + 2\phi_{n,m} + k_x\xi + k_y\zeta - \omega_n\tau]_0^{2\pi}$$

$$= \sum_n \sum_m \frac{A_{n,m}^2}{2} \cos\left(k_x\xi + k_y\zeta - \omega_n\tau\right)$$

The energy in the waves is found by $R(0,0,0) = \sum_n \sum_m \frac{A_{n,m}^2}{2}$. Recall that for a real process we have $R(-\xi,-\zeta,-\tau) = R(\xi,\zeta,\tau)$ and it follows that the spectrum has the symmetry $S\left(-k_x,-k_y,-\omega\right) = S\left(k_x,k_y,\omega\right)$. Furthermore the normalization criterion has to be satisfied:

$$\frac{1}{2}\int_{-\infty}^{\infty}\int_{k_x}\int_{k_y} S\left(k_x,k_y,\omega\right)\, dk_y\, dk_x\, d\omega = R(0,0,0)$$

$$\Rightarrow \quad \int_0^{\infty} S(\omega)\ d\omega = \sum_n \sum_m \frac{A_{n,m}^2}{2} \tag{1}$$

3.2 Directional spectrum

Directional spectrum describes the energy distribution in possible directions and is given by the following form:

$$D(\theta) = \begin{cases} \frac{1}{\beta}\cos^2\frac{\pi\theta}{2\beta} & |\theta| \le \beta \\ 0 & \end{cases} \qquad \text{[4] (2)}$$

Where β is the directional spreading coefficient, it infects the crest length of waves.

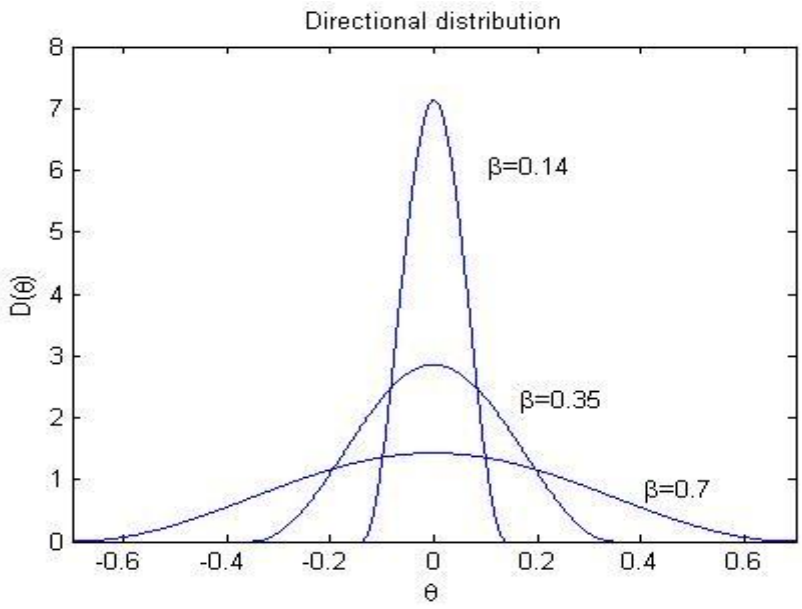

Figure 3.1: Directional distribution for 2D waves

Equation (2) has the following property:

$$\int_0^{\beta} D(\theta)d\theta = 1 \tag{3}$$

By multiplying (1) (3) together, we get:

$$\int_0^{\infty}\int_0^{2\pi} S(\omega)D(\theta)\,d\theta\,d\omega = \sum_n\sum_m \frac{A_{n,m}^2}{2}$$

Numerically, the amplitudes are found by:

$$A_{n,m} = \sqrt{2S(\omega)D(\theta)\Delta\omega\Delta\theta} \tag{4}$$

This analysis replaces the unknown spectrum $S(k_x, k_y, \omega)$ with two independent variables $S(\omega), D(\theta)$. Thus, it is only a simplification of the original spectrum.

3.3 Construction of the ocean surface elevation

Matlab code for generating 2D ocean surface waves is:

```
%Parameters.
alpha1=0.08;
alpha2=0.74;
g=9.8;
omegaP=?;
%Discretize omega.
d_omega=0.5;
omega_max=10;
omega_min=0.5;
omega=omega_min:d_omega:omega_max;
J=(omega_max-omega_min)/d_omega+1;
%Create the spectrum.
S=((alpha1*g^2)./omega.^5).*exp(-alpha2.*(omegaP./omega).^4);
%Discretize theta.
beta=?;
d_theta=0.05;
theta_max=beta2;
theta_min=-beta2;
theta=[theta_min:d_theta:theta_max]';
K=(theta_max-theta_min)/d_theta+1;
%Create the directional spectrum.
D=1/beta*(cos(pi*theta/(2*beta))).^2;
F=D*S;
%Amplitude of the 3D ocean wave.
A=sqrt(F*d_omega*d_theta);
%Discretization of time.
T=25;
dt=0.5;
Nt=T/dt;
t=0:dt:T-dt;
```

```
%Discretization of spatial length in x-direction.
Lx=20;
dx=0.2;
Nx=Lx/dx;
x=0:dx:Lx-dx;
%Discretization of spatial length in y-direction.
Ly=20;
dy=0.2;
Ny=Ly/dy;
y=0:dy:Ly-dy;
%construct wave numbers in both directions
[xx,yy,tt]=meshgrid(x,y,t);
kx=cos(theta)*omega.^2/g;
ky=sin(theta)*omega.^2/g;
%Generation of 2D ocean surface waves.
eta=0;
for k=1:K
    for j=1:J
       eta_frag=A(k,j)*sin(kx(k,j)*xx+ky(k,j)*yy-omega(j)*tt+2*pi*rand(1));
        eta=eta+eta_frag;
    end
end
surf(x,y,eta(:,:,1),'EdgeColor','none');
```

Since β effects the crest length, the appearance of the ocean surface changes with its value. For example, when $\beta = 0.75$, we get short-crested ocean waves:

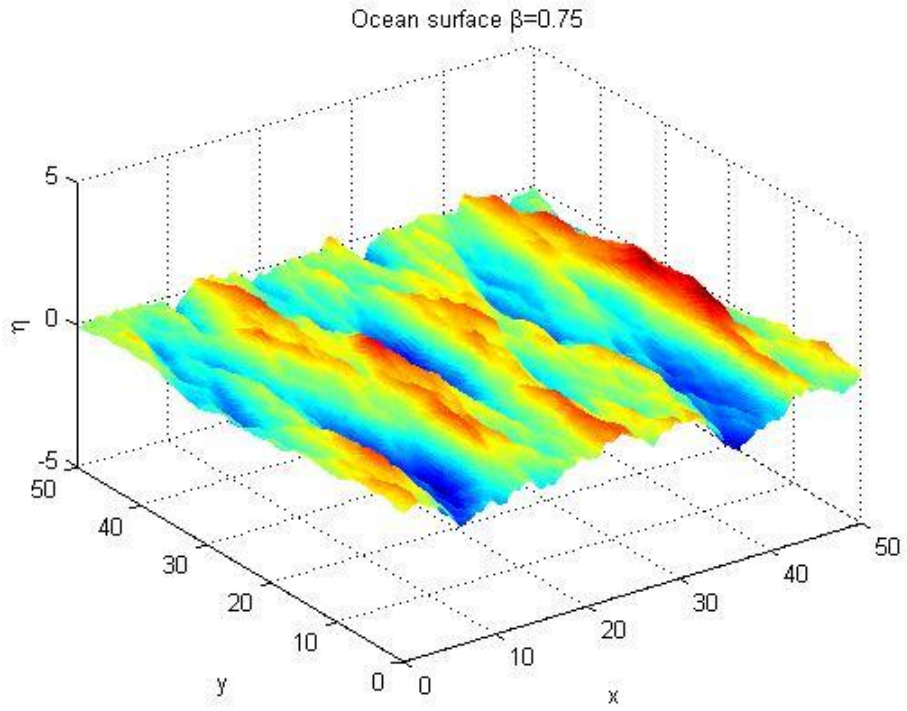

Figure 3.2: short crested ocean waves

When β number becomes a little bit smaller, say 0.35 we get long-crested waves.

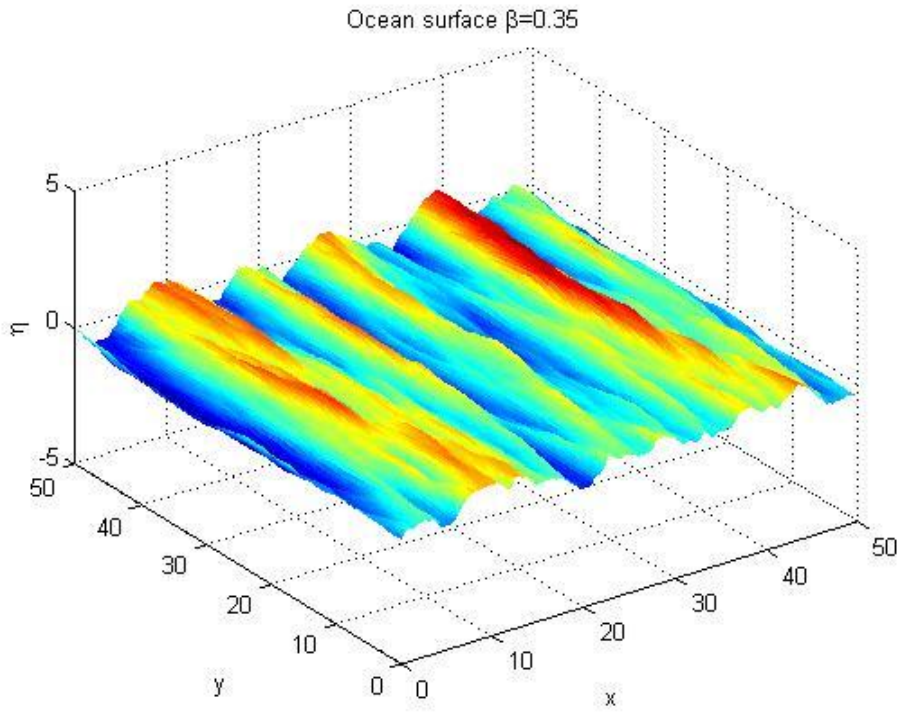

Figure 3.3: long crested ocean waves

As we decrease the number to very near to 0, the waves have infinite crest lengths.

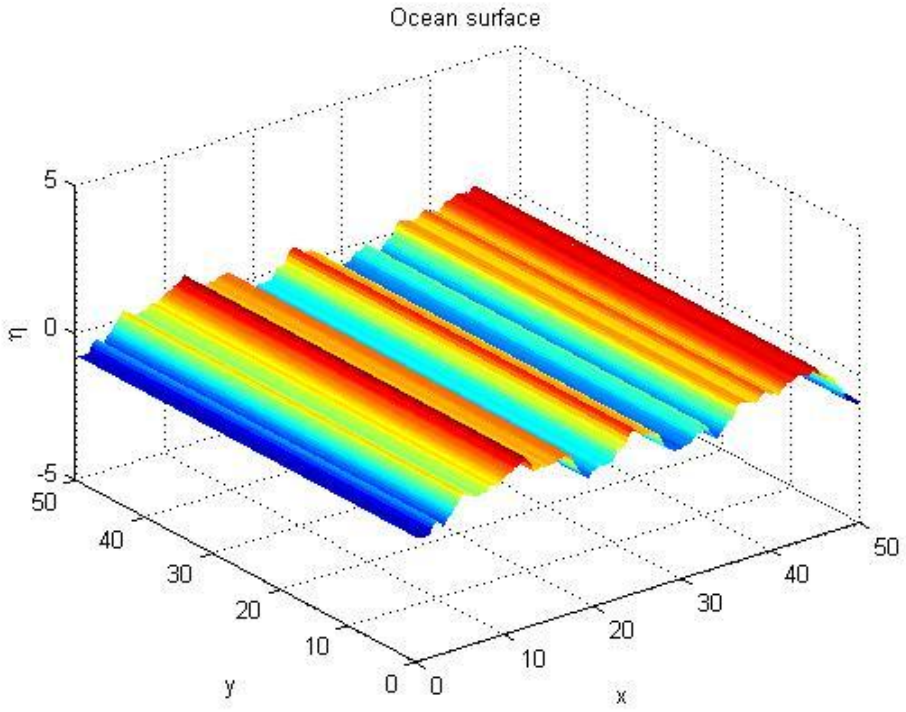

Figure 3.4: infinite long crested ocean waves

In conclusion, 2D wave model can be generated by introducing the directional spectrum. In the real ocean, the β number is around 0.15 up to 0.75, and the plots above look very realistic.

3.4 Algorithm & computation of the shadow masks

We shall establish a mathematical model for finding the shadow masks in several steps.

Step 1: Represent the line-function that light reflects from a random point $(a, b, \eta(a, b))$ on ocean surface to a spatially fixed observer $(0,0, h)$ over the surface. We define the line-function in 3D space to be $l_{a,b}$ and it is given by:

$$\frac{x}{a} = \frac{y}{b} = \frac{z - h}{\eta(a, b) - h} = p$$

$$\rightarrow x = ap;\ y = bp;\ z = (\eta(a, b) - h)p + h \qquad (5)$$

Step 2: Linearly discretize the space by sampling p from 0 to1 with I indices($p_1 = 0, \dots, p_I = 1$). So expression (5) becomes:

$$x_i = ap_i;\ y_i = bp_i;\ z_i = (c - h)p_i + h\ ;\quad i \in [1, I] \qquad (6)$$

Notice that $\{(x, y, z) | x = x_i;\ y = y_i;\ z \in R\}$determines almost a vertical plane going through the line-function $l_{a,b}$ so we define the plane to be $s_{a,b}$.

Step 3: Define the surface elevation function framed in the plane $s_{a,b}$ to be $\eta_{a,b}(x_i, y_i)$ and compare its values with $l_{a,b}(x_i, y_i)$. That is to check if:

$$\eta_{a,b}(x_i, y_i)\ \geq l_{a,b}(x_i, y_i)\ ;\ \ for\ any\ i = 1, \dots, I \qquad (7)$$

If condition (7) is satisfied, then the selected point $\eta(a, b)$ can not be observed by the radar.

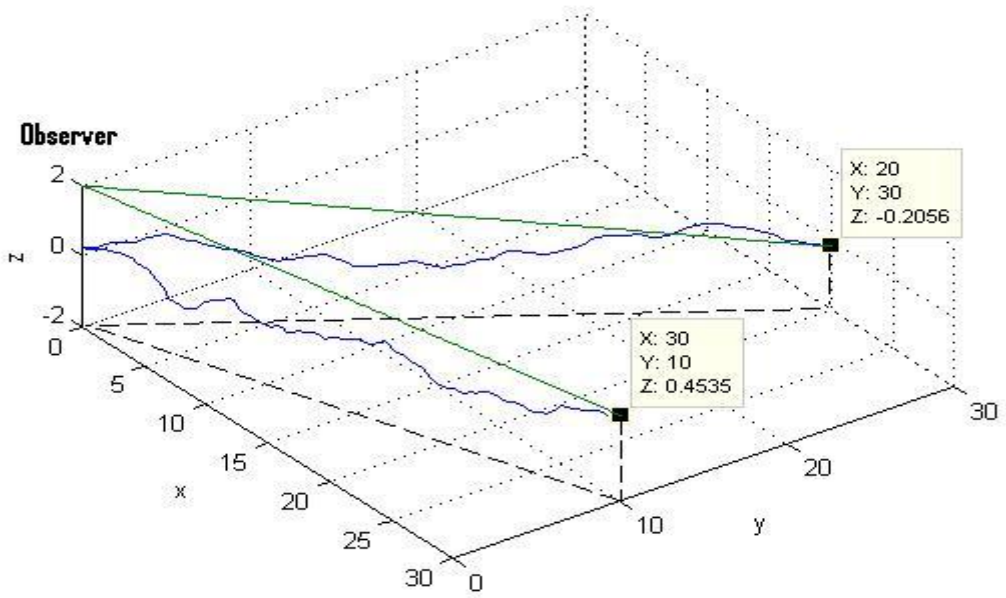

Figure 3.5: 2D shadow mask analysis

Make examples with two given points $\eta(20,30)$ and $\eta(30,10)$ on ocean surface (see figure 3.5). For the former point, we can observe from the figure that: In the plane $s_{20,30}$, there is at least one point on the ocean surface prevents the light from reaching the observer, which is consistent with condition (7), therefore the former point is invisible to the observer. For the later point, we can observe that: In the plane $s_{30,10}$, all points on the ocean surface are not able to block the light from its traveling to the radar, which is inconsistent with condition (7), therefore the later one is visible to the observer.

Implement the mathematical model with Matlab code:

```
function sm()
%Discretize omega.
d_omega=0.5;
omega_max=10;
omega_min=0.5;
omega=omega_min:d_omega:omega_max;
J=(omega_max-omega_min)/d_omega+1;
%Discretize theta.
beta2=0.35;
d_theta=0.05;
theta_max=beta2;
theta_min=-beta2;
theta=[theta_min:d_theta:theta_max]';
K=(theta_max-theta_min)/d_theta+1;
% Create phase shifts in advance
for n=1:K
    for m=1:J
        phi(n,m)=2*pi*rand(1);
    end
end
%Discretize spatial and time domain.
Lx=40;
Ly=50;
T=25;
x=0:1:Lx;
xn=length(x);
y=0:1:Ly;
yn=length(y);
t=0:0.5:T;
tn=length(t);
sm(xn,yn,tn)=1;
for k=1:tn
    fprintf('Time step %i of %i.\n',k,tn);
    for i=1:yn
        for j=1:xn
            sm(i,j,k)=Line(x(j),y(i),t(k),phi);
        end
    end
end
save('shadowmask_3d','sm','Lx','Ly','T');

%Find the line function
function sm=Line(x0,y0,t0,phi)
l=0:0.01:1;
x=x0*l;
y=y0*l;
eta0=eta3(x0,y0,t0,phi);
z=(eta0-2)*l+2;
eta=eta3(x,y,t0,phi);
```

```
v=z-eta;
sm=1;
for i=1:length(v)-1
    if v(i)<=0
        sm=0;
        break;
    end
end
return;

function eta=eta3(xx,yy,tt,phi)
%Parameters.
alpha1=0.08;
alpha2=0.74;
g=9.8;
omegaP=?;
%Discretize omega.
d_omega=0.5;
omega_max=10;
omega_min=0.5;
omega=omega_min:d_omega:omega_max;
J=(omega_max-omega_min)/d_omega+1;
%Create the spectrum.
S=((alpha1*g^2)./omega.^5).*exp(-alpha2.*(omegaP./omega).^4);
%Discretize theta.
beta=?;
d_theta=0.05;
theta_max=beta2;
theta_min=-beta2;
theta=[theta_min:d_theta:theta_max]';
K=(theta_max-theta_min)/d_theta+1;
%Create the directional spectrum.
D=1/beta*(cos(pi*theta/(2*beta))).^2;
F=D*S;
%Amplitude of the 3D ocean wave.
A=sqrt(F*d_omega*d_theta);
%construct wave numbers in both directions
[xx,yy,tt]=meshgrid(x,y,t);
kx=cos(theta)*omega.^2/g;
ky=sin(theta)*omega.^2/g;
%Construct surface elevations
eta=0;
for k=1:K
    for j=1:J
        eta_frag=A(k,j)*sin(kx(k,j)*xx+ky(k,j)*yy-omega(j)*tt+2*phi(k,j));
        eta=eta+eta_frag;
    end
    %fprintf('%i/%i is finished\n',k,round(K));
end
return;
```

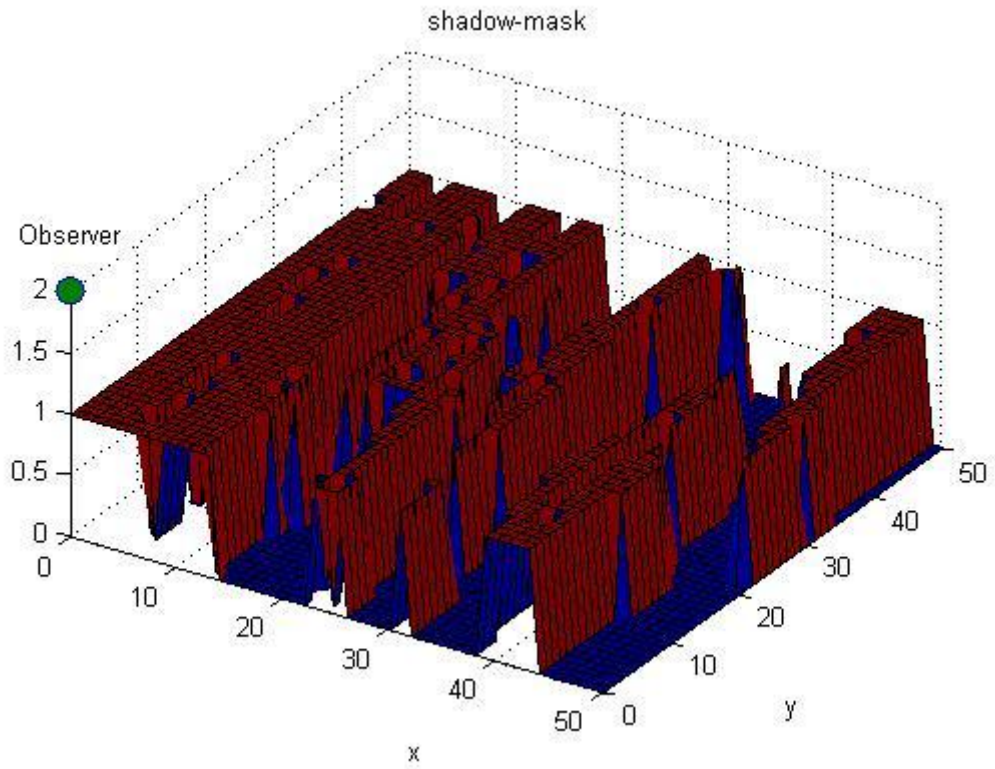

Figure 3.6: 2D shadow mask

The shadow mask in Figure 3.6 is observed from the radar at point (0,0,2). The red color represents ′1′s and the blue color represents '0's.

3.5 Wave and image spectra

Similar to the one dimensional case, the spectrum is considered as $\hat{S}(k_x, . k_y, \omega) = |\hat{\eta}(k_x, k_y, \omega)|^2$. Since the spectrum contains three variables- k_x,k_y and ω, a 3D contour plot of it reveal the dispersion relation of the original wave.

In Matlab, the discrete Fourier transform in a multi-dimensional space is implemented as:

$$Y = fft(X, [], dim) \text{ and } Y = fft(X, n, dim)$$

applies the FFT operation across the dimension dim.

And the "zero-padding" is implimented as:

$$Y = fftshift(X, dim)$$

applies the fftshift operation along the dimension dim

Matlab code for revealing the wave spectra:

```
%fft
s=size(eta)
Nx=s(1);
Ny=s(2);
Nt=s(3);
eta_hat=1/(Nx*Ny)*ifft(fft(fft(eta,[],1),[],2),[],3);
eta_hat=fftshift(eta_hat);
eta_estimator=(abs(eta_hat)).^2;
size(eta_estimator)
%re-construct omega for plots.
n_omega=0:Nt-1;
omega2=2*pi*(n_omega-round(Nt/2))/T;
%re-construct kx for plots.
n_kx=0:Nx-1;
kx2=2*pi*(n_kx-round(Nx/2))/Lx;
%re-construct ky for plots.
n_ky=0:Ny-1;
ky2=2*pi*(n_ky-round(Ny/2))/Ly;

%create meshgrids for k and omega.
[ky,kx,omega]=meshgrid(ky2,kx2,omega2);
size(kx)

[kx3 ky3]=meshgrid(kx2,ky2);
surf(kx3,ky3,sqrt(9.8*sqrt(kx3.^2+ky3.^2)),'edgecolor','none');hold on;

isosurface(ky,kx,omega,eta_estimator,0.005);
xlabel('k_x');ylabel('k_y');zlabel('\omega');
```

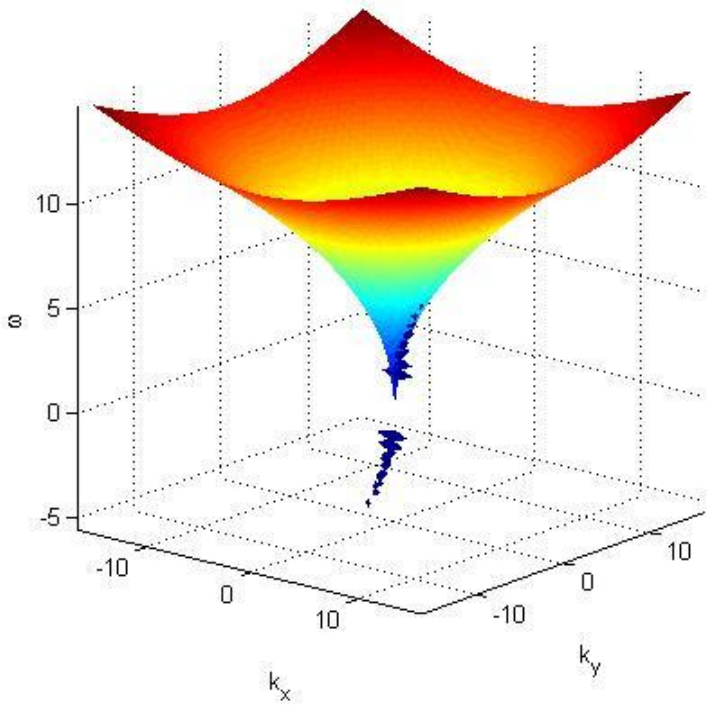

Figure 3.7: wave spectra of 2D ocean surface waves

In figure 3.7, the colored, curved surface is the dispersion shell for the gravity waves $\omega = \sqrt{g\sqrt{k_x^2 + k_y^2}}$ in infinitely deep water. The contour plot is symmetric around the origin and part of the contour lies along the theoretical dispersion function.

Similarly, we compute the Fourier transform $\widehat{Sm}(k_x, k_y, \omega)$ of the shadow masks $Sm(x, y, t)$, and the image spectrum becomes $\hat{I}(k_x, k_y, \omega) = \left|\widehat{Sm}(k_x, k_y, \omega)\right|^2$.

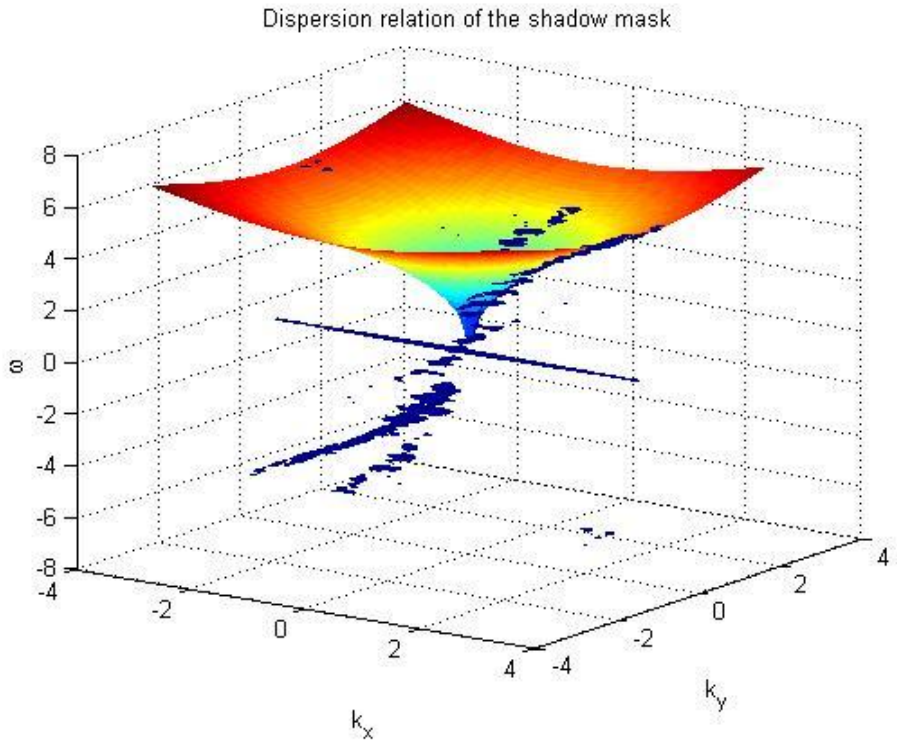

Figure 3.8: Image spectra of the shadow masks in 2D

In figure 3.8, the contours lie dispersed along different harmonic shells including the 0th, the 1st and the 2nd ones. There are infinitely many harmonic shells and they are all partly occupied by these contours. By comparing figure 3.8 with figure 3.7, we also notice that the image spectra mantle the wave spectra, in other words, the image spectra contain useful information of the waves.

Chapter 4

1D, 2nd order ocean surface waves

4.1 Derivation of 2nd order wave surface elevation

Equations for an incompressible, in-viscid fluid:

$$\frac{\partial \eta}{\partial t} + \frac{\partial \phi}{\partial x}\frac{\partial y}{\partial x} = \frac{\partial \phi}{\partial z} \quad at\ z = \eta \tag{1}$$

$$\frac{\partial \phi}{\partial t} + g\eta + \frac{1}{2}(\nabla \phi)^2 = 0 \quad at\ z = \eta \tag{2}$$

$$\nabla^2 \phi = 0 \quad for -\infty < z < \eta \tag{3}$$

Introduce perturbation expansions to the second order:

$$\eta = \epsilon \eta_1 + \epsilon^2 \eta_2 \tag{4}$$

$$\phi = \epsilon \phi_1 + \epsilon^2 \phi_2 \tag{5}$$

Set (4), (5) into (1):

$$\epsilon\left(\frac{\partial\eta_1}{\partial t}-\frac{\partial\phi_1}{\partial z}\right)+\epsilon^2\left(\frac{\partial\eta_2}{\partial t}+\frac{\partial\phi_1}{\partial x}\frac{\partial\eta_1}{\partial x}-\frac{\partial\phi_2}{\partial z}\right)+\epsilon^3\left(\frac{\partial\phi_2}{\partial x}\frac{\partial\eta_1}{\partial x}+\frac{\partial\phi_1}{\partial x}\frac{\partial\eta_2}{\partial x}\right)+\epsilon^4\frac{\partial\phi_2}{\partial x}\frac{\partial\eta_2}{\partial x}=0 \tag{6}$$

Set (4), (5) into (2):

$$\epsilon\left(\frac{\partial\phi_1}{\partial t}+g\eta_1\right)+\epsilon^2\left[\frac{\partial\phi_2}{\partial t}+g\eta_2+\frac{1}{2}\left(\frac{\partial\phi_1}{\partial x}\right)^2+\frac{1}{2}\left(\frac{\partial\phi_1}{\partial z}\right)^2\right]+\epsilon^3\left(\frac{\partial\phi_1}{\partial x}\frac{\partial\phi_2}{\partial x}+\frac{\partial\phi_1}{\partial z}\frac{\partial\phi_2}{\partial z}\right)+\epsilon^4\left[\frac{1}{2}\left(\frac{\partial\phi_2}{\partial x}\right)^2+\frac{1}{2}\left(\frac{\partial\phi_2}{\partial z}\right)^2\right]=0 \tag{7}$$

Set (4), (5) into (3):

$$\epsilon\left(\frac{\partial^2\phi_1}{\partial x^2}+\frac{\partial^2\phi_1}{\partial z^2}\right)+\epsilon^2\left(\frac{\partial^2\phi_2}{\partial x^2}+\frac{\partial^2\phi_2}{\partial z^2}\right)=0 \tag{8}$$

Separate $O(\epsilon)$ for (η_1,ϕ_1), equations (6)-(8) become:

$$\frac{\partial\eta_1}{\partial t}-\frac{\partial\phi_1}{\partial z}=0 \quad at\ z=\eta \tag{9}$$

$$\frac{\partial\phi_1}{\partial t}+g\eta_1=0 \quad at\ z=\eta \tag{10}$$

$$\frac{\partial^2\phi_1}{\partial x^2}+\frac{\partial^2\phi_1}{\partial z^2}=0 \quad for\ -\infty<z<\eta \tag{11}$$

Assume a particular set of solutions for equations (9)-(11):

$$\eta_1^p=Re\left\{A\,e^{i(kx-\omega t)}\right\} \tag{12}$$

$$\phi_1^p=Re\left\{B\,e^{|k|z}\,e^{i(kx-\omega t)}\right\} \tag{13}$$

The absolute sign prevents an exponential growth in the potential function. And equation (13) guarantees that the potential tends to be 0 at infinite water depth $z = -\infty$.

Set (12), (13) into (9), and evaluate the equation at $z = 0$:

$$-i\omega A\, e^{i(kx-\omega t)} - kBe^{|k|z}\, e^{i(kx-\omega t)} = 0$$

$$\rightarrow B = -\frac{i\omega A}{k} \tag{14}$$

Set (12), (13) into (10), and evaluate the equation at $z = 0$:

$$-i\omega Be^{kz}\, e^{i(kx-\omega t)} + gAe^{i(kx-\omega t)} = 0$$

$$\rightarrow B = \frac{Ag}{i\omega} \tag{15}$$

From (14), (15), we can get the dispersion relation for deep water (infinite water depth):

$$\omega^2 = kg \tag{16}$$

Due to the linearity of the equations (9)-(11), the summation of all the particular solutions is the general solution, so we seek solution of the following form:

$$\eta_1 = \sum_n Re\left\{A_n e^{i(k_n x-\omega_n t)}\right\} \tag{17}$$

$$\phi_1 = \sum_n Re\left\{B_n\, e^{|k_n|z}\, e^{i(k_n x-\omega_n t)}\right\} \tag{18}$$

Where $B_n = \frac{A_n g}{i\omega}$.

Separate $O(\epsilon^2)$ for (η_2, ϕ_2), equations (6)-(8) become:

$$\frac{\partial \eta_2}{\partial t} - \frac{\partial \phi_2}{\partial z} + \frac{\partial \phi_1}{\partial x}\frac{\partial \eta_1}{\partial x} = 0 \quad at\ z = \eta \tag{19}$$

$$\frac{\partial \phi_2}{\partial t} + g\eta_2 + \frac{1}{2}\left(\frac{\partial \phi_1}{\partial x}\right)^2 + \frac{1}{2}\left(\frac{\partial \phi_1}{\partial z}\right)^2 = 0 \quad at\ z = \eta \tag{20}$$

$$\frac{\partial^2 \phi_2}{\partial x^2} + \frac{\partial^2 \phi_2}{\partial z^2} = 0 \quad for\ -\infty < z < \eta \tag{21}$$

First of all, we calculate the following expressions:

$$\frac{\partial \phi_1}{\partial x} = \sum_n Re\left\{iB_n k_n e^{|k_n|z}\ e^{i(k_n x - \omega_n t)}\right\} \tag{22}$$

$$\frac{\partial \phi_1}{\partial z} = \sum_n Re\left\{B_n |k_n| e^{|k_n|z}\ e^{i(k_n x - \omega_n t)}\right\} \tag{23}$$

$$\frac{\partial \eta_1}{\partial x} = \sum_n Re\left\{iA_n k_n e^{i(k_n x - \omega_n t)}\right\} \tag{24}$$

By the bi-chromatic identity, we get:

$$\begin{aligned}&\frac{\partial \phi_1}{\partial x}\frac{\partial \eta_1}{\partial x}\\&=\sum_n\sum_m Re\{iA_nk_ne^{i(k_nx-\omega_nt)}\}Re\{iB_mk_me^{|k_m|z}\,e^{i(k_mx-\omega_mt)}\}\\&=\sum_n\sum_m Re\{-A_nB_mk_nk_me^{|k_m|z}e^{i[(k_n+k_m)x-(\omega_n+\omega_m)t]}\\&-A_nB_mk_nk_me^{|k_m|z}e^{i[(k_n-k_m)x-(\omega_n-\omega_m)t]}\}\end{aligned}\tag{25}$$

$$\begin{aligned}&\left(\frac{\partial \phi_1}{\partial x}\right)^2\\&=\sum_n\sum_m Re\{iB_nk_ne^{|k_n|z}\,e^{i(k_nx-\omega_nt)}\}Re\{iB_mk_me^{|k_m|z}\,e^{i(k_mx-\omega_mt)}\}\\&=\sum_n\sum_m Re\{-B_nB_mk_nk_me^{|k_n|z}e^{|k_m|z}e^{i[(k_n+k_m)x-(\omega_n+\omega_m)t]}\\&-B_nB_mk_nk_me^{|k_n|z}e^{|k_m|z}e^{i[(k_n-k_m)x-(\omega_n-\omega_m)t]}\}\end{aligned}\tag{26}$$

$$\begin{aligned}&\left(\frac{\partial \phi_1}{\partial z}\right)^2\\&=\sum_n\sum_m Re\{B_n|k_n|e^{|k_n|z}\,e^{i(k_nx-\omega_nt)}\}Re\{B_m|k_m|e^{|k_m|z}\,e^{i(k_mx-\omega_mt)}\}\\&=\sum_n\sum_m Re\{B_nB_m|k_n||k_m|e^{|k_n|z}e^{|k_m|z}e^{i[(k_n+k_m)x-(\omega_n+\omega_m)t]}\\&+B_nB_m|k_n||k_m|e^{|k_n|z}e^{|k_m|z}e^{i[(k_n-k_m)x-(\omega_n-\omega_m)t]}\}\end{aligned}\tag{27}$$

Set the expressions (25)-(27) into the equations (19)-(20) and we get:

$$\begin{aligned}&\frac{\partial \eta_2}{\partial t}-\frac{\partial \phi_2}{\partial z}\\&=\sum_n\sum_m Re\{A_nB_mk_nk_me^{|k_m|z}e^{i[(k_n+k_m)x-(\omega_n+\omega_m)t]}\\&+A_nB_mk_nk_me^{|k_m|z}e^{i[(k_n-k_m)x-(\omega_n-\omega_m)t]}\}\end{aligned}\tag{28}$$

$$
\begin{aligned}
&\frac{\partial \phi_2}{\partial t} + g\eta_2 \\
&= \frac{1}{2}\sum_n \sum_m Re\{B_n B_m k_n k_m e^{|k_n|z} e^{|k_m|z} e^{i[(k_n+k_m)x-(\omega_n+\omega_m)t]} \\
&+ B_n B_m k_n k_m e^{|k_n|z} e^{|k_m|z} e^{i[(k_n-k_m)x-(\omega_n-\omega_m)t]}\} \\
&- \frac{1}{2}\sum_n \sum_m Re\{B_n B_m |k_n||k_m| e^{|k_n|z} e^{|k_m|z} e^{i[(k_n+k_m)x-(\omega_n+\omega_m)t]} \\
&+ B_n B_m |k_n||k_m| e^{|k_n|z} e^{|k_m|z} e^{i[(k_n-k_m)x-(\omega_n-\omega_m)t]}\}
\end{aligned}
\tag{29}
$$

To simplify the equations, we want to get rid of the potential function. Take time derivative of equation (28) and z-derivative of equation (29) on both sides, we get:

$$
\begin{aligned}
&\frac{\partial^2 \eta_2}{\partial t^2} - \frac{\partial^2 \phi_2}{\partial z \partial t} \\
&= \sum_n \sum_m Re\{-i(\omega_n + \omega_m) A_n B_m k_n k_m e^{|k_m|z} e^{i[(k_n+k_m)x-(\omega_n+\omega_m)t]} \\
&\qquad - i(\omega_n - \omega_m) A_n B_m k_n k_m e^{|k_m|z} e^{i[(k_n-k_m)x-(\omega_n-\omega_m)t]}\}
\end{aligned}
\tag{30}
$$

$$
\begin{aligned}
&\frac{\partial^2 \phi_2}{\partial t \partial z} + \frac{g \partial \eta_2}{\partial z} \\
&= \frac{1}{2}(|k_n| + |k_m|)\sum_n \sum_m Re\{B_n B_m k_n k_m e^{|k_n|z} e^{|k_m|z} e^{i[(k_n+k_m)x-(\omega_n+\omega_m)t]} \\
&\qquad + B_n B_m k_n k_m e^{|k_n|z} e^{|k_m|z} e^{i[(k_n-k_m)x-(\omega_n-\omega_m)t]}\} \\
&- \frac{1}{2}(|k_n| + |k_m|)\sum_n \sum_m Re\{B_n B_m |k_n||k_m| e^{|k_n|z} e^{|k_m|z} e^{i[(k_n+k_m)x-(\omega_n+\omega_m)t]} \\
&\qquad + B_n B_m |k_n||k_m| e^{|k_n|z} e^{|k_m|z} e^{i[(k_n-k_m)x-(\omega_n-\omega_m)t]}\}
\end{aligned}
\tag{31}
$$

Equation (30) + (31) gives:

$$
\frac{\partial^2 \eta_2}{\partial t^2} + g\frac{\partial \eta_2}{\partial z} \tag{32}
$$

$$= \sum_n \sum_m Re\left\{\left[-i(\omega_n + \omega_m)A_n B_m k_n k_m e^{|k_m|z} + \frac{1}{2}(|k_n| + |k_m|)B_n B_m k_n k_m e^{|k_n|z} e^{|k_m|z} - \frac{1}{2}(|k_n| + |k_m|)B_n B_m |k_n||k_m| e^{|k_n|z} e^{|k_m|z}\right] e^{i[(k_n+k_m)x-(\omega_n+\omega_m)t]}\right\}$$

$$+ \sum_n \sum_m Re\left\{\left[-i(\omega_n - \omega_m)A_n B_m k_n k_m e^{|k_m|z} + \frac{1}{2}(|k_n| + |k_m|)B_n B_m k_n k_m e^{|k_n|z} e^{|k_m|z} - \frac{1}{2}(|k_n| + |k_m|)B_n B_m |k_n||k_m| e^{|k_n|z} e^{|k_m|z}\right] e^{i[(k_n-k_m)x-(\omega_n-\omega_m)t]}\right\}$$

Assume a solution to equation (32) of the following form:

$$\eta_2 = \sum_n \sum_m Re\left\{C_{n,m}^S e^{i[(k_n+k_m)x-(\omega_n+\omega_m)t]}\right\} + \sum_n \sum_m Re\left\{C_{n,m}^D e^{i[(k_n-k_m)x-(\omega_n-\omega_m)t]}\right\} \quad (33)$$

Set (33) into (32) and the left hand side of equation (32) becomes:

$$\frac{\partial^2 \eta_2}{\partial t^2} + g\frac{\partial \eta_2}{\partial z}$$

$$= \sum_n \sum_m Re\left\{-C_{n,m}^S(\omega_n + \omega_m)^2 e^{i[(k_n+k_m)x-(\omega_n+\omega_m)t]}\right\} + \sum_n \sum_m Re\left\{-C_{n,m}^D(\omega_n - \omega_m)^2 e^{i[(k_n-k_m)x-(\omega_n-\omega_m)t]}\right\} \quad (34)$$

Compare equation (34) with (32), and evaluate them at $z = 0$:

$$C_{n,m}^S(\omega_n + \omega_m)^2 = i(\omega_n + \omega_m)A_n B_m k_n k_m + \frac{1}{2}B_n B_m(|k_n| + |k_m|)(|k_n||k_m| - k_n k_m)$$

$$\rightarrow C_{n,m}^{S} = i\frac{A_n B_m k_n k_m}{(\omega_n + \omega_m)} + \frac{B_n B_m (|k_n| + |k_m|)(|k_n||k_m| - k_n k_m)}{2(\omega_n + \omega_m)^2} \tag{35}$$

$$C_{n,m}^{D}(\omega_n - \omega_m)^2 = i(\omega_n - \omega_m) A_n B_m k_n k_m + \frac{1}{2} B_n B_m (|k_n| + |k_m|)(|k_n||k_m| - k_n k_m)$$

$$\rightarrow C_{n,m}^{D} = i\frac{A_n B_m k_n k_m}{(\omega_n - \omega_m)} + \frac{B_n B_m (|k_n| + |k_m|)(|k_n||k_m| - k_n k_m)}{2(\omega_n - \omega_m)^2} \tag{36}$$

In the case of only positive wave numbers are concerned, we have much simplified expressions:

$$C_{n,m}^{S} = i\frac{A_n B_m k_n k_m}{(\omega_n + \omega_m)} \tag{37}$$

$$C_{n,m}^{D} = i\frac{A_n B_m k_n k_m}{(\omega_n - \omega_m)} \tag{38}$$

Set expression (15) into (37), (38), we get:

$$C_{n,m}^{S} = \frac{g A_n A_m k_n k_m}{\omega_m(\omega_n + \omega_m)} \tag{39}$$

$$C_{n,m}^{D} = \frac{g A_n A_m k_n k_m}{\omega_m(\omega_n - \omega_m)} \tag{40}$$

We notice that the expressions (39), (40) are only valid when $\omega_n \neq \omega_m$. In the case of $\omega_n = \omega_m$, the second term of expression (33) is only a constant, and it gives no contribution after taking the derivative of t and z. Therefore, the only coefficient left is $C_{n,n}^{S}$:

$$C_{n,n}^{S} = \frac{g A_n^2 k_n^2}{2\omega_n^2} \tag{41}$$

Set the dispersion relation for infinitely deep water (16) to expression (41):

$$C_{n,n}^{S} = \frac{1}{2} k_n A_n^2 \tag{42}$$

The final expressions for the second order ocean surface waves in infinitely deep water are:

When $\omega_m \neq \omega_n$	$\eta_2 = \sum_n \sum_m Re\left\{\frac{g A_n A_m k_n k_m}{\omega_m(\omega_n + \omega_m)} e^{i[(k_n+k_m)x-(\omega_n+\omega_m)t]}\right\} + \sum_n \sum_m Re\left\{\frac{g A_n A_m k_n k_m}{\omega_m(\omega_n - \omega_m)} e^{i[(k_n-k_m)x-(\omega_n-\omega_m)t]}\right\}$	(43)
When $\omega_m = \omega_n$	$\eta_2 = \sum_n Re\left\{\frac{1}{2} k_n A_n^2 e^{2i(k_n x-\omega_n t)}\right\}$	(44)

4.2 Construction of the 2nd order wave surface elevation

The following Matlab code describes equation (43), (44) numerically.

```
%Construct the wave elevation.
function eta2(L,T,M,N,omegaP,filename)
%L-spatial length;
%T-time length;
%M-num. of spatial points;
%N-num. of time points;
%omegaP-peak wave frequency in PM-spectrum
alpha=0.0081;
beta=0.74;
g=9.8;
%Discretize omega.
d_omega=0.2;
omega_max=6;
omega_min=0.2;
omega=omega_min:d_omega:omega_max;
J=(omega_max-omega_min)/d_omega+1;
%calculate the wave number.
k=omega.^2/g;
%Create the spectrum.
S=((alpha*g^2)./omega.^5).*exp(-beta.*(omegaP./omega).^4);
```

```
%Construct the coefficients Aj.
A=sqrt(2*S*d_omega);
%Discretize the time and spatial domain.
dt=T/N;
dx=L/M;
[x,t]=meshgrid(0:dx:L-dx,0:dt:T-dt);
%load phase
structure=load('phase','-mat');
phi=structure.phi;
%Construct the wave elevation.
eta=0;
for j=1:J
    eta_frag=A(j)*cos(k(j)*x-
omega(j)*t+phi(j))+1/2*A(j)^2*(omega(j)^2/g)*cos(2*omega(j)^2/g*x-
2*omega(j)*t+2*phi(j));
    eta=eta+eta_frag;
end
for j1=1:J
    for j2=1:J
        if j1~=j2

eta_frag=g*A(j1)*A(j2)*k(j1)*k(j2)/(omega(j2)*(omega(j1)+omega(j2)))*cos((k
(j1)+k(j2))*x-
(omega(j1)+omega(j2))*t+phi(j1)+phi(j2))+g*A(j1)*A(j2)*k(j1)*k(j2)/(omega(j
2)*(omega(j1)-omega(j2)))*cos((k(j1)-k(j2))*x-(omega(j1)-
omega(j2))*t+phi(j1)-phi(j2));
            eta=eta+eta_frag;
        end
    end
end
x=x(1,:);t=t(:,1)';
save(filename,'x','t','eta','L','T');
fprintf('Sea surface creation is done.\n');
```

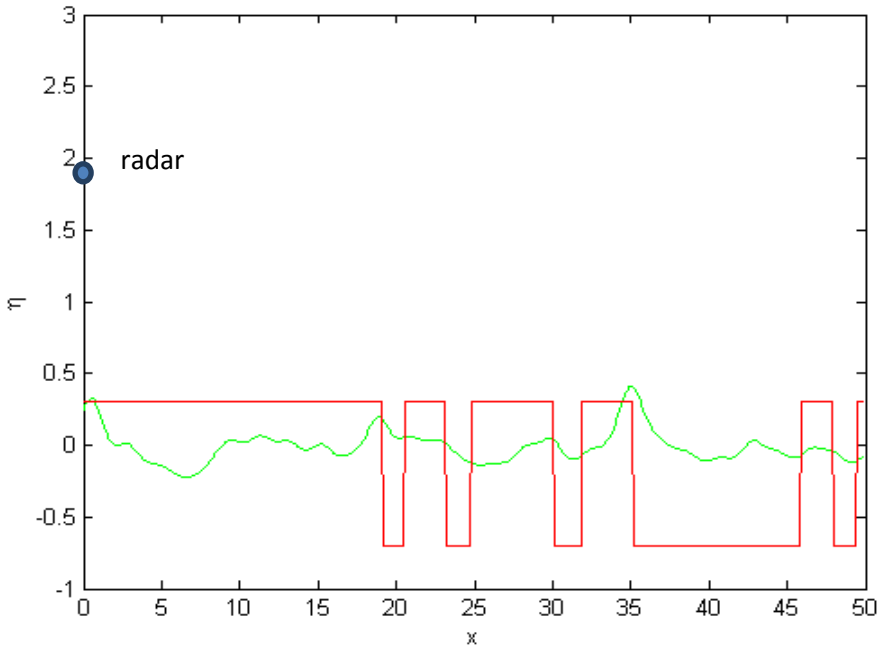

Figure 4.1: The 2nd order ocean wave field (green) and its shadow mask (red)

4.3 Wave and image spectra

I

With the same method introduced in Chapter 2.7, we can extract the wave spectra of the 2nd order wave field. Notice that the plot should be made in logarithmic scales rather than in linear ones, otherwise some parts of the contours are too small in values to be visible.

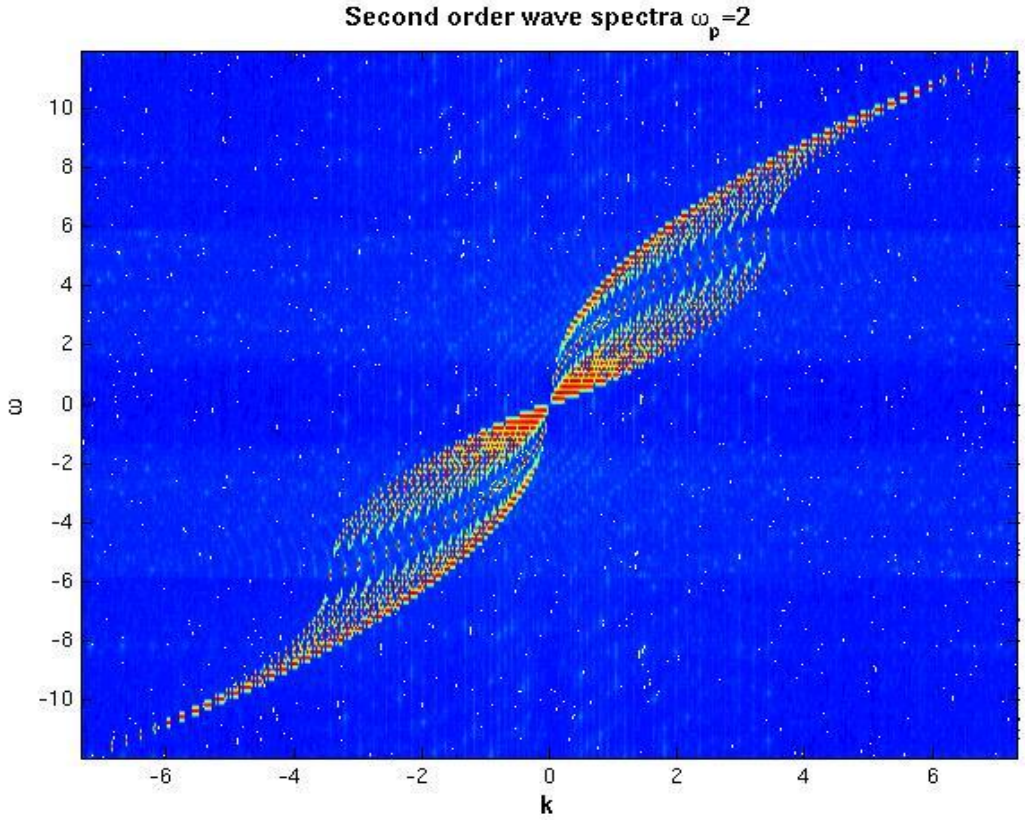

Figure 4.2 second order wave spectra

From Figure 4.2, we observe four contours with different locations. The flat circular shaped contour centered around the 0th harmonic shell is generated by the second term of equation (43); The thin, parabolic shaped contour on the 1st harmonic (dispersion shell) is generated by the linear waves; The parabolic shaped contour on the 2nd harmonic is generated by equation (44); And the wing shaped contour between the 1st and 2nd harmonics is generated by the first term of equation (43).

We are also interested in two more plots: image spectra to the 1st order linear wave field and the 2nd order nonlinear wave field. See the following plots:

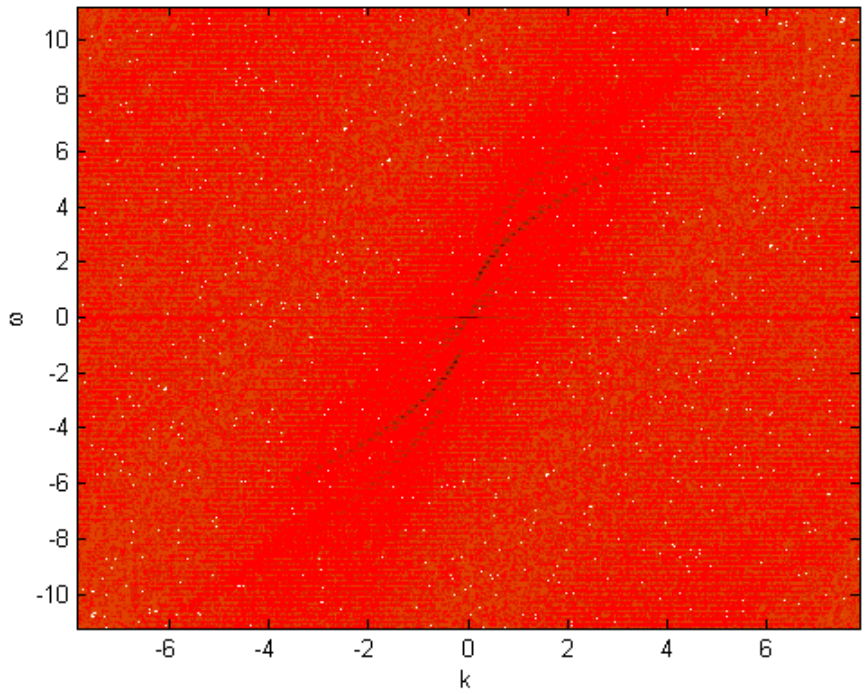

Figure 4.3 Image spectra of shadow masks for the 1st order linear wave field.

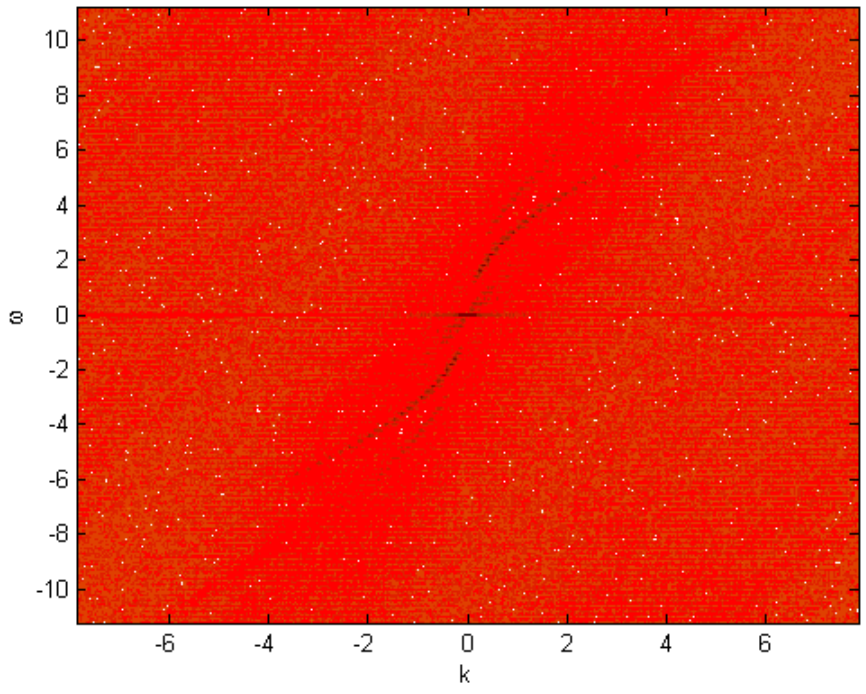

Figure 4.4 Image spectra of shadow masks for the 2nd order nonlinear wave field.

By comparing Figure 4.3 with Figure 4.4, we understand that there is no big difference in appearance of the two image spectra. For the 1st order image spectra (Figure 4.3), the energy on the 2nd harmonic shell is complete noise generated by the nonlinearity of the shadow masks, but for the 2nd order image spectra, the energy on the same shell contains both noise and wave information. Then the problem arises: How can we extract the wave information from the noise on the 2nd harmonic shell?

4.4 Extract wave information from shadow masks

In this section, we aim to extract wave information from Fourier analysis of shadow masks with special attention to the 2nd harmonic shell. Therefore, we consider the following wave functions:

$$\eta_{1st} = \sum_{i=1}^{N} A_i \cos(k_i x - \omega_i t + \phi_i) \tag{45}$$

$$\eta_{2nd} = \sum_{i=1}^{N} [A_i \cos(k_i x - \omega_i t + \phi_i) + \frac{1}{2} A_i^2 k_i \cos(2k_i x - 2\omega_i t + 2\phi_i)] \tag{46}$$

Equation (46) is a simplification of the 2nd order ocean waves according to the analysis in section 4.2. The reason of doing this is to consider the energy only on the 2nd harmonic shell. My numerical experiments showed different appearances of the image spectra with respect to ω_p (defined in section 2.3)

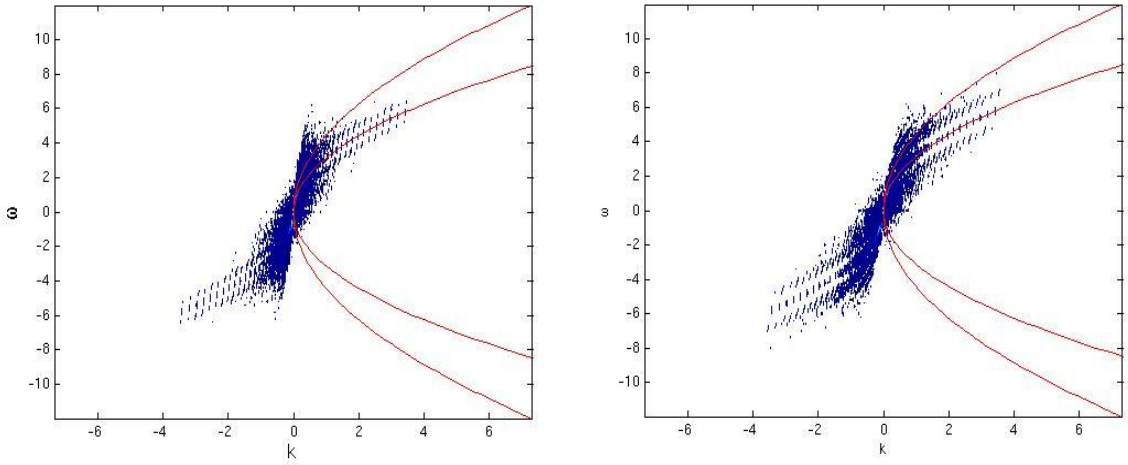

Figure 4.5 Image spectra of shadow masks with $\omega_p = 0.6$ (left) and $\omega_p = 1$(right)

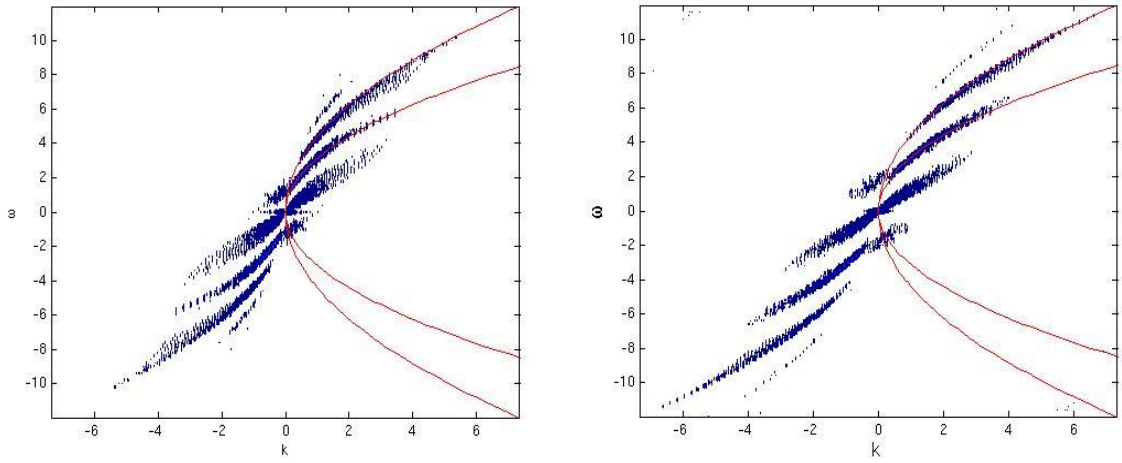

Figure 4.6 Image spectra of shadow masks with $\omega_p = 2$ (left) and $\omega_p = 3$(right)

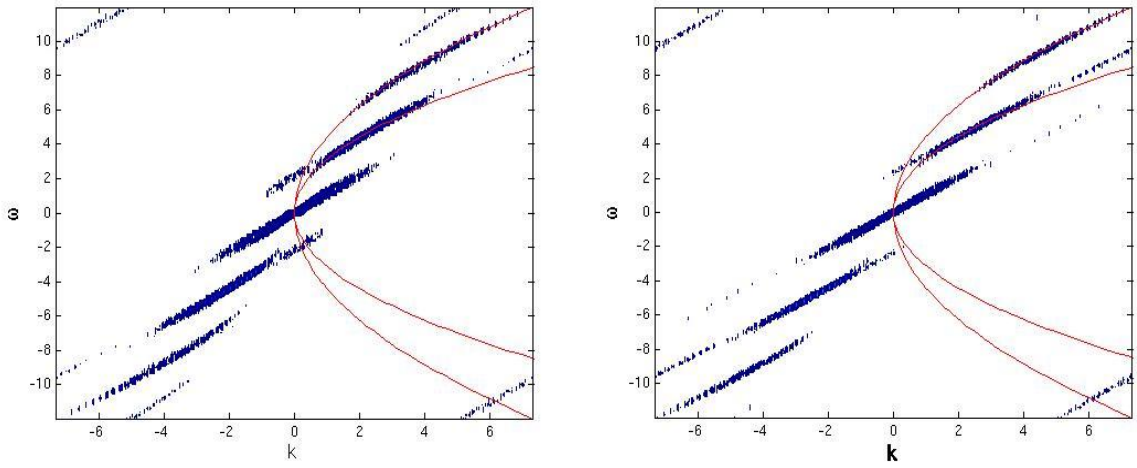

Figure 4.7 Image spectra of shadow masks with $\omega_p = 4$ (left) and $\omega_p = 5$(right)

From Figure 4.5 to 4.7, we observe that: as the significant wave height gets smaller (ω_p gets bigger), the contours spread out from the center to harmonic shells and gradually become tangent to the shells. The theory for the experiments is introduced in the next section.

Wave height estimation from image spectra is based on an empirical formula $H_s = A + B\sqrt{SNR}$, where H_s is the estimated significant wave height, SNR is the signal-to-noise ratio, and A, B are two empirical parameters that can usually only be determined by a field experimental calibration campaign. For synthetic data generated by numerical experiments, the signal-to-noise ratio is the wave information divided by the information of shadowing. The wave information is traditionally considered as the energy on the harmonic shells (except the 0th harmonic shell). However, this is not completely correct. For the 2nd order image spectra, both the wave information (signal) and the information of shadowing (noise) are contained on the 2nd harmonic shell. Theoretically, a wrong signal-to-noise ratio can cause an inaccurate result in the estimation of the significant wave height. Therefore, how to distinguish the signal from the noise on the shell is of our interest. A possible way of achieving the goal is to make a comparison of the 1st and 2nd order image spectra, that is to compare the energy on the 2nd harmonic shell of the 1st order image spectra (only noise) with that of the 2nd order one (signal and noise). So we shall filter out the energy on the 2nd harmonic shell for both cases. A traditional filtering method is to take a bunch of energy within a certain bandwidth along the 2nd harmonic shell. However, this method is very inaccurate after looking closely to figure 4.5. When the ocean surface is at a violent state (wave height is big), noise-energy dots outside the 2nd harmonic shell are too close to the shell and they are much bigger in values.

In order to get reliable results, it is necessary to allocate each energy dot in exact one cell along the 1st and 2nd harmonic shells. This thought can be carried out by taking the advantage of the dispersion relation. In infinitely deep water, the 1st and 2nd harmonic shells are $\omega^2 = gk$ and $\frac{\omega^2}{2} = gk$ respectively. A suggested discrete frequency range for ocean surfaces is $0.3 < \omega < 6.0$ $(1.7m < \lambda < 685m)$[5]. I expand the range a little bit farther, from 0.2 to 6.0, and a series of calculations are carried out to find a proper solution for this matter.

For the 1st harmonic shell:

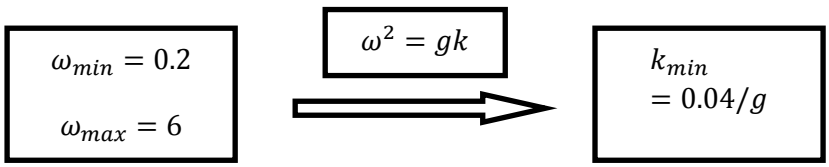

For the 2nd harmonic shell:

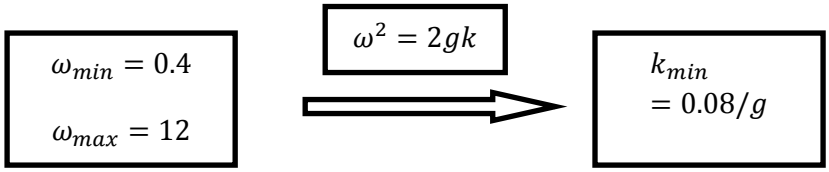

This indicates that if each energy dot on the 1st harmonic shell is located in exact one cell, so does that on the 2nd harmonic shell. Furthermore, the spatial and time length taken should cover the extra wave number range ($\omega \in (6,12]$) and the extra frequency range ($k \in (36/g, 72/g]$) on the 2nd harmonic shell. It is also suggested that the frequency is discretized in steps of $\Delta\omega = 0.05$ [5]. However, this tiny value of the step-length would consume massive time in computations, which is very hard for school computers. To spend an acceptable time in computations, I choose to discretize the frequency in steps $\Delta\omega = 0.2$, and therefore get the following statistics on the 1st harmonic.

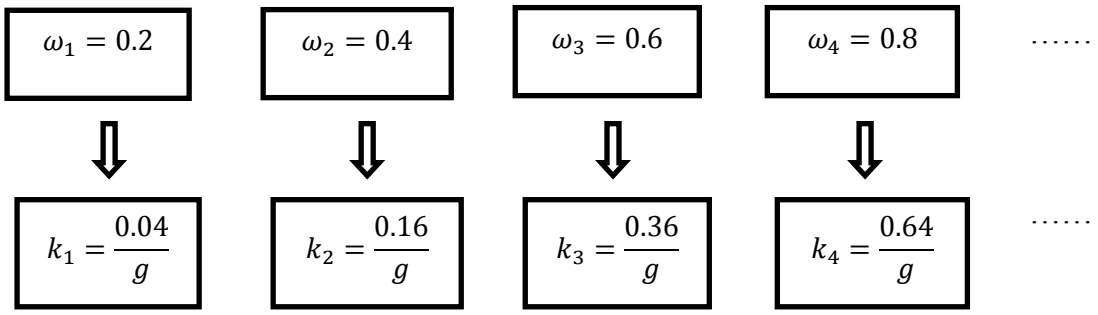

The above suggests us the following discretization:

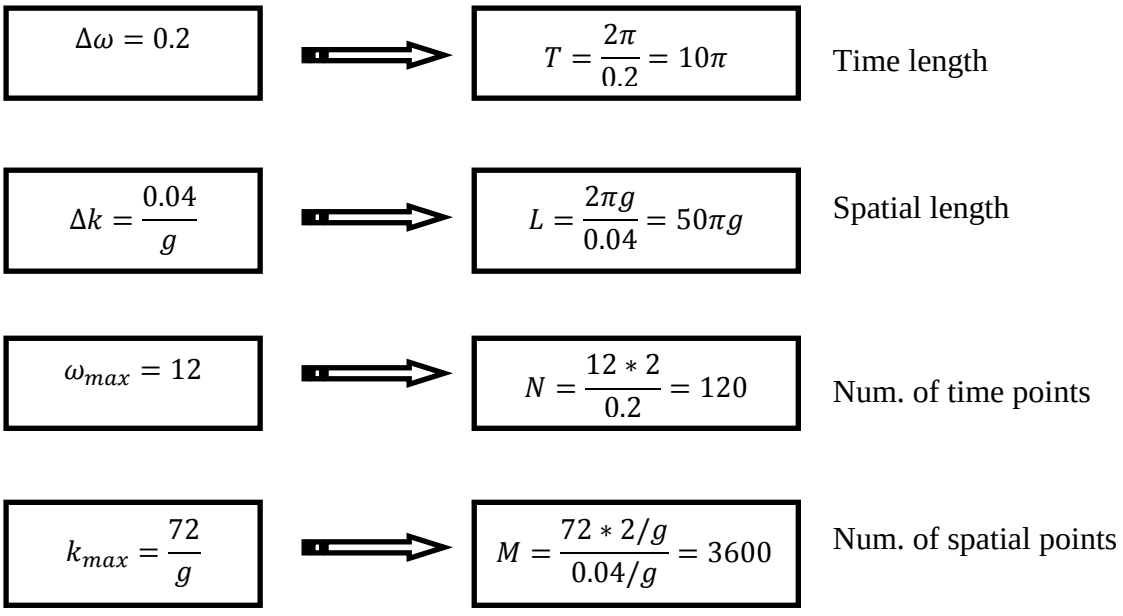

The above four parameters are used as inputs of the numerical code to generate the 1st and 2nd order ocean waves and their shadow masks. The rest of the work is to track the frequencies and wave numbers in pair along the two shells and filter them out. The following two plots are a proof of the success.

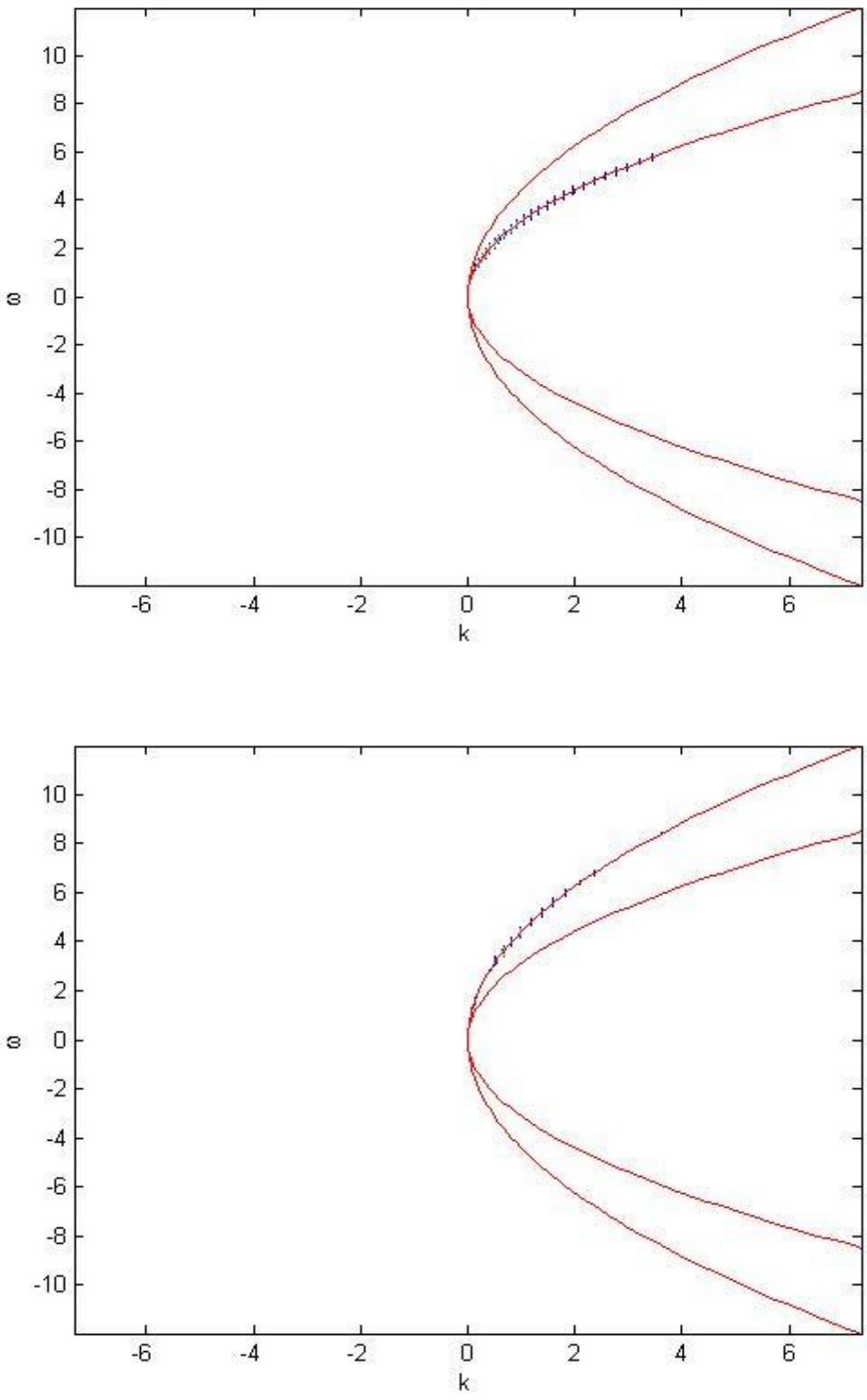

Figure 4.5: Filtered energy on the 1st and 2nd harmonic shells.

And the following two tables contain the statistics collected from the numerical experiments with $g = 9.8(m/s^2)$.

4.5 The statistics of image spectrum for both 1st and 2nd order ocean waves with radar height 10(m), spatial length $50\pi g$(m) and time length 10π(s).

ωp	0.4	0.6	0.8	1.0	1.2	1.4	1.6	1.8	2.0	2.2	2.4	2.6	2.8	3.0
Hs1	12.5199	5.6170	3.2431	2.0544	1.4295	1.0494	0.8027	0.6335	0.5123	0.4224	0.3539	0.3004	0.2578	0.2232
Hs2	12.5260	5.6186	3.2437	2.0547	1.4297	1.0495	0.8028	0.6336	0.5123	0.4224	0.3539	0.3004	0.2578	0.2232
D1	15.4783	22.5121	26.9115	30.6971	34.0451	36.8514	39.5721	42.5036	45.3933	48.1320	50.6809	53.0851	55.0851	57.9340
D2	15.1697	22.2536	26.7572	30.5391	33.8735	36.7298	39.4749	42.2647	45.1491	47.9817	50.5321	52.9858	55.5809	57.7695
F1	2.3391	0.8438	0.5198	0.5088	0.3319	0.4312	0.5178	0.5088	0.4497	0.4064	0.3902	0.3574	0.3268	0.3017
F2	2.6066	1.0247	0.6409	0.6367	0.4658	0.5806	0.6493	0.6345	0.5673	0.5179	0.4904	0.4564	0.4177	0.4037
E1	118.026	131.125	139.000	146.107	152.486	158.624	164.690	170.685	175.946	181.190	186.133	190.892	195.626	199.905
E2	117.463	130.758	138.722	145.808	152.175	158.453	164.523	170.477	175.732	181.043	185.981	190.810	195.510	199.843

Hs1 *represents the significant wave height of the* 1^{st} *order ocean wave generated by PM-spectrum.*
Hs2 *represents the significant wave height of the* 2^{nd} *order ocean wave generated by PM-spectrum.*
D1 *represents the energy on the* 1^{st} *harmonic shell of the* 1^{st} *order ocean wave image spectrum.*
D2 *represents the energy on the* 1^{st} *harmonic shell of the* 2^{nd} *order ocean wave image spectrum.*
F1 *represents the energy on the* 2^{nd} *harmonic shell of the* 1^{st} *order ocean wave image spectrum.*
F2 *represents the energy on the* 2^{nd} *harmonic shell of the* 2^{nd} *order ocean wave image spectrum.*
E1 *represents the total energy of the* 1^{st} *order ocean wave image spectrum.*
E2 *represents the total energy of the* 2^{nd} *order ocean wave image spectrum.*
ωp *represents the peak wave frequency in the PM-spectrum.*

The statistics of image spectrum for both 1st and 2nd order ocean waves

with radar height 25(m), spatial length $50\pi g$(m) and time length 10π(s).

ωp	**0.4**	**0.6**	**0.8**	**1.0**	**1.2**	**1.4**	**1.6**	**1.8**	**2.0**	**2.2**	**2.4**	**2.6**	**2.8**	**3.0**
Hs1	12.5199	5.6170	3.2431	2.0544	1.4295	1.0494	0.8027	0.6335	0.5123	0.4224	0.3539	0.3004	0.2578	0.2232
Hs2	12.5260	5.6186	3.2437	2.0547	1.4297	1.0495	0.8028	0.6336	0.5123	0.4224	0.3539	0.3004	0.2578	0.2232
D1	48.6608	53.8744	56.3767	59.4576	61.5543	63.5024	65.6453	67.2866	68.1993	68.8693	69.5287	69.9141	69.7031	69.1269
D2	48.3486	53.7044	56.0855	59.2160	61.2985	63.2621	65.5193	67.1506	67.9445	68.7539	69.4040	69.8143	69.6284	69.0233
F1	1.8107	0.5019	0.4540	0.3828	0.4285	0.3476	0.2893	0.2312	0.2194	0.1936	0.1738	0.1579	0.1517	0.1469
F2	2.0537	0.7647	0.6848	0.6068	0.6350	0.5008	0.4110	0.3424	0.3300	0.2955	0.2602	0.2395	0.2328	0.2104
E1	192.700	199.585	205.134	209.653	213.211	216.080	218.338	219.986	220.985	221.405	221.235	220.477	219.081	217.056
E2	192.458	199.422	204.930	209.522	213.096	215.997	218.307	219.968	220.962	221.403	221.245	220.500	219.110	217.080

Hs1 *represents the significant wave height of the 1^{st} order ocean wave generated by PM-spectrum.*
Hs2 *represents the significant wave height of the 2^{nd} order ocean wave generated by PM-spectrum.*
D1 *represents the energy on the 1^{st} harmonic shell of the 1^{st} order ocean wave image spectrum.*
D2 *represents the energy on the 1^{st} harmonic shell of the 2^{nd} order ocean wave image spectrum.*
F1 *represents the energy on the 2^{nd} harmonic shell of the 1^{st} order ocean wave image spectrum.*
F2 *represents the energy on the 2^{nd} harmonic shell of the 2^{nd} order ocean wave image spectrum.*
E1 *represents the total energy of the 1^{st} order ocean wave image spectrum.*
E2 *represents the total energy of the 2^{nd} order ocean wave image spectrum.*
ωp *represents the peak wave frequency in the PM-spectrum.*

4.6 Analysis of the results

Ideally, if $E1 = E2$, the energy difference $F2 - F1$ would represent the wave energy (wave information) on the 2nd harmonic shell of the 2nd order ocean waves. However, in our case, the total energy ($E1$ and $E2$) are not equal due to the unequal wave heights ($Hs1$ and $Hs2$). Since the difference is very small, I use a correction-factor on $F1$ so as to get a more accurate result:

$$wave\ energy\ on\ the\ 2nd\ \ harmonic = F2 - \frac{E2}{E1}F1 \quad (46)$$

After applying this method, we find out three important information:

1) The wave energy on the 2nd harmonic tends to get bigger as the wave height gets higher.
2) The wave energy on the 2nd harmonic is much smaller than the noise-energy on the same shell.
3) The wave energy on the 1st harmonic gets smaller as the wave height gets higher.

The Calibration method [6] suggests that the significant wave height of the 2nd order ocean waves can be determined by:

$$Hs = a\sqrt{\frac{D2 + F2}{E2 - D2 - F2}} + b \quad (47)$$

Since the formula miss-uses $F2$ as the wave energy input ($F2 - \frac{E2}{E1}F1$), the acuracy of Hs measured can be very different in two cases. (See table 2)

Case 1: The sea is peaceful (Significant wave height is small)

In this case, we have:

$$F2\ (around\ 0.2) \ll D2(around\ 70)$$
$$F2 - \frac{E2}{E1}F1\ (around\ 0.07) \ll D2(around\ 70)$$

So the replacement of $F2 - \frac{E2}{E1}F1$ with $F2$ does not affect the significant wave height much. Thus, the formula is pretty accurate.

Case 2: The sea is violent (Significant wave height is big)

In this case, we have:

$$F2\ (around\ 2)\ is\ comparible\ to\ D2(around\ 48)$$
$$F2 - \frac{E2}{E1}F1\ (around\ 0.2) \ll D2(around\ 48)$$

So the miss-use of $F2$ would cause an inaccurate wave height. From this point of view, the more violent sea becomes, the less accurate Hs becomes.

Chapter 5

Wave field generated by the NLS equation and its shadowing effects

5.1 Solving the NLS equation with split step Fourier method.

We shall limit our consideration to solving the cubic nonlinear Schrödinger (NLS) equation for deep water of infinite depth. The NLS equation is given as:

$$\frac{\partial A}{\partial t} + c_g \frac{\partial A}{\partial x} + \frac{ic_g}{4k_c}\frac{\partial^2 A}{\partial x^2} + \frac{i}{2}\omega_c k_c^2 |A|^2 A = 0 \qquad [7](1)$$

Step 1: Scale the equation with dimensionless variables.

Introduce the following dimensionless variables:

$$t^* = \omega_c t; \qquad x^* = k_c x; \qquad A^* = k_c A$$

Equation (1) then becomes:

$$\frac{\partial A^*}{\partial t^*} + \frac{1}{2}\frac{\partial A^*}{\partial x^*} + \frac{i}{8}\frac{\partial^2 A^*}{\partial x^{*2}} + \frac{i}{2}|A^*|^2 A^* = 0 \qquad (2)$$

Step 2: Normalize the spatial domain.

The spatial domain is normalized from $x \in [0, L)$ to $X = [0,2\pi)$ by setting $X = \frac{2\pi}{L}x$.

Equation (2) then becomes (replace $x^* \ with \ x$ for convinience):

$$i\frac{\partial A}{\partial t} = -\frac{i\pi}{L}\frac{\partial A}{\partial x} + \frac{\pi^2}{2L^2}\frac{\partial^2 A}{\partial x^2} + \frac{1}{2}|A|^2 A \qquad (3)$$

Step 3: Use split step Fourier method. [8]

Let the linear part and non-linear part on the right hand side of equation (3) to be:

$$-\frac{i\pi}{L}\frac{\partial}{\partial x}+\frac{\pi^2}{2L^2}\frac{\partial^2 A}{\partial x^2}=\widehat{D}\,; \qquad \frac{1}{2}|A|^2=\widehat{N}$$

And equation (3) becomes:

$$i\frac{\partial A}{\partial t}=\left[\widehat{D}+\widehat{N}\right]A \tag{4}$$

Equation (4) has the general solution:

$$A(x,t)=e^{-it[\widehat{D}+\widehat{N}]}A(x,0) \tag{5}$$

Since $\left[\widehat{D}+\widehat{N}\right]$ are operators, they do not in general commute. However, the Baker-Hausdroff formula showed that the error from treating them as if they do is of order $O(dt^2)$. Therefore we write:

$$A(x,t+dt)=e^{-idt\widehat{D}}e^{-idt\widehat{N}}A(x,t) \tag{6}$$

Apply Fourier transformation on both sides of equation (6) and the partial derivative operator can be converted into a number by substituting im for $\frac{\partial}{\partial x}$, where $m=-\frac{M}{2},\dots,-1,0,1,\dots,\frac{M}{2}-1$ and M is the number of spatial grids. [9]Then we have:

$$F[A(x,t+dt)]=F\left[e^{-idt\widehat{D}}e^{-idt\widehat{N}}A(x,t)\right]$$

$$\rightarrow F[A(x,t+dt)]=e^{-idt[-\frac{i\pi}{L}(im)+\frac{\pi^2}{2L^2}(im)^2]}F\left[e^{-idt\widehat{N}}A(x,t)\right]$$

$$\rightarrow F[A(x,t+dt)]=e^{-idt[\frac{\pi}{L}m-\frac{\pi^2}{2L^2}m^2]}F\left[e^{-idt\frac{1}{2}|A|^2}A(x,t)\right] \tag{7}$$

Use inverse Fourier transformation on both sides of equation (7) *again* we get:

$$A(x,t+dt)=F^{-1}\left[e^{-idt[\frac{\pi}{L}m-\frac{\pi^2}{2L^2}m^2]}F\left[e^{-idt\frac{1}{2}|A|^2}A(x,t)\right]\right] \tag{8}$$

Step 4: Reconstruct the surface elevation to the 2nd order.

For the dimensional surface

$$\eta(x,t)=\frac{1}{2}\left[A(x,t)e^{i(k_c x-\omega_c t)}+\frac{1}{2}k_c A(x,t)^2 e^{i(k_c x-\omega_c t)}+c.c\right] \tag{9}$$

For the dimensionless surface:

$$\eta^*(x^*,t^*)=\frac{1}{2}[A^*(x^*,t^*)e^{i(x^*-t^*)}+\frac{1}{2}A^*(x^*,t^*)^2e^{i(x^*-t^*)}+c.c] \quad (10)$$

Where $c.c$ represents the complex conjugates for the previous two terms.

Matlab code for step 1-step 4:

```
function nls11(kc,M,N)
%discretize the dimensionless spatial distance and time interval.
L=500;
T=250;
dx=L/(M);
dt=T/(N);
x=0:dx:(M-1)*dx;
t=0:dt:(N-1)*dt;
%initial condition
%Function initial1() can only deal with dimensional quantities: the
%parameters it carries and the value it returns are all dimensional.
%initial1() is introduced in Step5 later.
A=kc*initial1(x/kc,kc);
%Split step Fourier method.
m = -M/2:1:M/2-1;
for n=1:N
    A=exp(-i*0.5*abs(A).^2*dt).*A;
    A=fftshift(fft(A));
    A=exp(-i*dt*(pi/(L)*m-pi^2/(2*L^2)*m.^2)).*A;
    A=ifft(fftshift(A));
    Q(:,n)=A;
end
%construct the 2nd order dimensionless surface elevation.
Q2=1/2*Q.^2;
for t_j=1:N
    for x_j=1:M
        eta(x_j,t_j)=0.5*(Q(x_j,t_j)*exp(i*(x(x_j)-
t(t_j)))+conj(Q(x_j,t_j))*exp(-i*(x(x_j)-
t(t_j)))+Q2(x_j,t_j)*exp(2*i*(x(x_j)-t(t_j)))+conj(Q2(x_j,t_j))*exp(-
2*i*(x(x_j)-t(t_j))));
    end
end
%for plots and other uses.
A=Q;
save('111','x','t','A','eta','dx','dt','kc');
eta=eta';
save('data','x','t','eta','L','T','kc');
```

5.2 Derivation of the spectrum of the amplitude.

The amplitude $A(x,t)$is a complex quantity; it is of the following form:

$$A(x,t) = \sum_n B_n e^{i(k_n x - \omega_n t + \phi_n)}$$

where ϕ_n is a random variable from [0, 2π).The auto-correlation function is then (* here represents the complex conjugate):

$$R_A(\xi) = E[A(x,t)A^*(x+\xi,t)]$$

$$= E\left[\left(\sum_n B_n e^{i(k_n x - \omega_n t + \phi_n)}\right)\left(\sum_m B_m e^{-i(k_m x + k_m \xi - \omega_m t + \phi_m)}\right)\right]$$

Set $\theta_n = k_n x - \omega_n t + \phi_n$ and $\alpha_m = k_m \xi$, we get:

$$= E\left[\sum_n \sum_m B_n B_m e^{i(\theta_n - \theta_m - \alpha_m)}\right]$$

$$= E\left[\sum_n \sum_m B_n B_m e^{i\theta_n} e^{-i\theta_m} e^{-i\alpha_m}\right]$$

$$= \sum_n \sum_m B_n B_m E\left[e^{i\theta_n} e^{-i\theta_m} e^{-i\alpha_m}\right]$$

$$= \sum_n B_n^2 E\left[e^{-i\alpha_n}\right]$$

$$= \sum_n B_n^2 e^{-ik_n\xi}$$

The spectrum of $A(x,t)$is the inverse Fourier transform of $R_A(\xi)$, so we have:

$$S_A(k) = \frac{1}{2\pi}\int_{-\infty}^{\infty} R_A(\xi)\, e^{-ik\xi} d\xi$$

$$= \frac{1}{2\pi}\int_{-\infty}^{\infty} \sum_n B_n^2 e^{-ik_n\xi}\, e^{-ik\xi} d\xi$$

$$= \sum_n B_n^2 \frac{1}{2\pi}\int_{-\infty}^{\infty} e^{-i(k+k_n)\xi} d\xi$$

Introducing Dirac delta function $\frac{1}{2\pi}\int_{-\infty}^{\infty} e^{\pm ix(a-\omega)} dx = \delta(\omega - a)$, we get:

	$$S_A(k) = \sum_n B_n^2 \delta(k + k_n)$$	(11)

5.3 Derivation of wave number spectrum for the 2nd order wave surface construction.

Set in $A(x,t) = \sum_n B_n e^{i(k_n x - \omega_n t + \phi_n)}$ and we get:

$$\eta(x,t) = \sum_n B_n \cos\{(k_n + k_c)x - (\omega_n + \omega_c)t + \phi_n\} + \frac{1}{2}\sum_n \sum_m B_n B_m k_c \cos\{(k_n + k_m + 2k_c)x - (\omega_n + \omega_m + 2\omega_c)t + \phi_n + \phi_m\}$$

The auto-correlation function is:

$$R_\eta(\xi) = E[\eta(x,t)\eta(x+\xi,t)]$$

$$= E\left[\left(\sum_n B_n \cos\{(k_n + k_c)x - (\omega_n + \omega_c)t + \phi_n\} + \frac{1}{2}\sum_n \sum_m B_n B_m k_c \cos\{(k_n + k_m + 2k_c)x - (\omega_n + \omega_m + 2\omega_c)t + \phi_n + \phi_m\}\right)\left(\sum_p B_p \cos\{(k_p + k_c)(x+\xi) - (\omega_p + \omega_c)t + \phi_p\} + \frac{1}{2}\sum_p \sum_q B_p B_q k_c \cos\{(k_p + k_q + 2k_c)(x+\xi) - (\omega_p + \omega_q + 2\omega_c)t + \phi_p + \phi_q\}\right)\right]$$

Let $\theta_n = (k_n + k_c)x - (\omega_n + \omega_c)t + \phi_n$ and $\alpha_n = (k_n + k_c)\xi$ and set them into equation (11), we get:

$$R_\eta(\xi) = E\left[\left(\sum_n B_n \cos\theta_n + \frac{1}{2}\sum_n \sum_m B_n B_m k_c \cos(\theta_n + \theta_m)\right)\left(\sum_p B_p \cos(\theta_p + \alpha_p) + \frac{1}{2}\sum_p \sum_q B_p B_q k_c \cos(\theta_p + \theta_q + \alpha_p + \alpha_q)\right)\right]$$

$$= E\left[\sum_n \sum_p B_n B_p \cos\theta_n \cos(\theta_p + \alpha_p) + \frac{1}{2}\sum_n \sum_m \sum_p B_n B_m B_p k_c \cos(\theta_n + \theta_m)\cos(\theta_p + \alpha_p) + \frac{1}{2}\sum_n \sum_p \sum_q B_n B_p B_q k_c \cos\theta_n \cos(\theta_p + \theta_q + \alpha_p + \alpha_q) + \frac{1}{4}\sum_n \sum_m \sum_p \sum_q B_n B_m B_p B_q k_c^2 \cos(\theta_n + \theta_m)\cos(\theta_p + \theta_q + \alpha_p + \alpha_q)\right]$$

Since $\theta_n, \theta_m, \theta_p, \theta_q$ are independent of each other, we have :

$$= E\left[\sum_n B_n^2 \cos\theta_n \cos(\theta_n + \alpha_n) + \frac{1}{2}\sum_n B_n^3 k_c \cos(2\theta_n)\cos(\theta_n + \alpha_n) + \frac{1}{2}\sum_n B_n^3 k_c \cos\theta_n \cos(2\theta_n + 2\alpha_n) + \frac{1}{4}\sum_n B_n^4 k_c^2 \cos(2\theta_n)\cos(2\theta_n + 2\alpha_n)\right]$$

we use the trigonometric formula $\frac{\cos(a+b)+\cos(a-b)}{2} = \cos a \cos b$ and get:

$$= E\left[\sum_n B_n^2 \frac{\cos(2\theta_n + \alpha_n) + \cos\alpha_n}{2} + \frac{1}{2}\sum_n B_n^3 k_c \frac{\cos(3\theta_n + \alpha_n) + \cos(\theta_n - \alpha_n)}{2} + \frac{1}{2}\sum_n B_n^3 k_c \frac{\cos(3\theta_n + 2\alpha_n) + \cos(\theta_n + 2\alpha_n)}{2} + \frac{1}{4}\sum_n B_n^4 k_c^2 \frac{\cos(4\theta_n + 2\alpha_n) + \cos 2\alpha_n}{2}\right]$$

$$= \sum_n E[B_n^2 \frac{\cos\alpha_n}{2} + \frac{1}{4} B_n^4 k_c^2 \frac{\cos 2\alpha_n}{2}]$$

$$= \frac{1}{2}\sum_n B_n^2 \cos\alpha_n + \frac{1}{8}\sum_n B_n^4 k_c^2 \cos 2\alpha_n$$

$$= \frac{1}{2}\sum_n B_n^2 \cos\{(k_n + k_c)\xi\} + \frac{1}{8}\sum_n B_n^4 k_c^2 \cos\{2(k_n + k_c)\xi\}$$

The wave spectrum is then:

$$S_\eta(k) = \frac{1}{2\pi}\int_{-\infty}^{\infty} R_\eta(\xi)\, e^{-ik\xi} d\xi$$

$$= \frac{1}{2\pi}\int_{-\infty}^{\infty}\left(\frac{1}{2}\sum_n B_n^2 \cos\{(k_n + k_c)\xi\} + \frac{1}{8}\sum_n B_n^4 k_c^2 \cos\{2(k_n + k_c)\xi\}\right) e^{-ik\xi} d\xi$$

Since $\cos\{(k_n + k_c)\xi\} = \frac{1}{2} e^{i(k_n + k_c)\xi} + \frac{1}{2} e^{-i(k_n + k_c)\xi}$, we get:

$$= \frac{1}{4}\sum_n B_n^2 \frac{1}{2\pi}\int_{-\infty}^{\infty}\left(e^{i(k_n + k_c - k)\xi} + e^{-i(k_n + k_c + k)\xi}\right) d\xi + \frac{1}{16}\sum_n B_n^4 k_c^2 \frac{1}{2\pi}\int_{-\infty}^{\infty}\left(e^{i(2k_n + 2k_c - k)\xi} + e^{-i(2k_n + 2k_c + k)\xi}\right) d\xi$$

Introducing Dirac delta function $\frac{1}{2\pi}\int_{-\infty}^{\infty} e^{\pm i\xi(a-k)} d\xi = \delta(k - a)$, we get:

	$S_\eta(k) = \frac{1}{4}\sum_n B_n^2 \{\delta(k - k_n - k_c) + \delta(k + k_n + k_c)\} + \frac{1}{16}\sum_n B_n^4 k_c^2 \{\delta(k - 2k_n - 2k_c) + \delta(k + 2k_n + 2k_c)\}$	(12)

5.4 Relationship between the wave spectrum and the amplitude spectrum.

We assume that B_n decreases as $n \to \pm\infty$, then the wave spectrum in equation (12) has four peaks allocated at $-2k_c, -k_c, k_c, 2k_c$ respectively (one-sided spectrum has only two peaks). As a result, many theoretical wave spectra like Pierson&Moskowitz spectrum, Jonswap spectrum, Gaussian spectrum are not consistent with the multiple peaks. Therefore, none of them is a good description of the actual wave spectrum if we insist on the nonlinear theory. How can we create a correct spectrum for the waves? Let us first investigate equation (11). We also assume that B_n decreases as $n \to \pm\infty$, then the amplitude spectrum in equation (11) has only one peak centered at $k_0 = 0$, which can be described by any of the theoretical spectra mentioned (P&M, Jonswap or Gaussian spectrum). In addition, the amplitude spectrum $S_A(k)$ is linked with the wave spectrum $S_\eta(k)$ by the constant factors B_n. This indicates that if we generate $S_A(k)$ with, for example Gaussian spectrum, then $S_\eta(k)$ will naturally be generated with multiple peaks. See Figure 5.1.

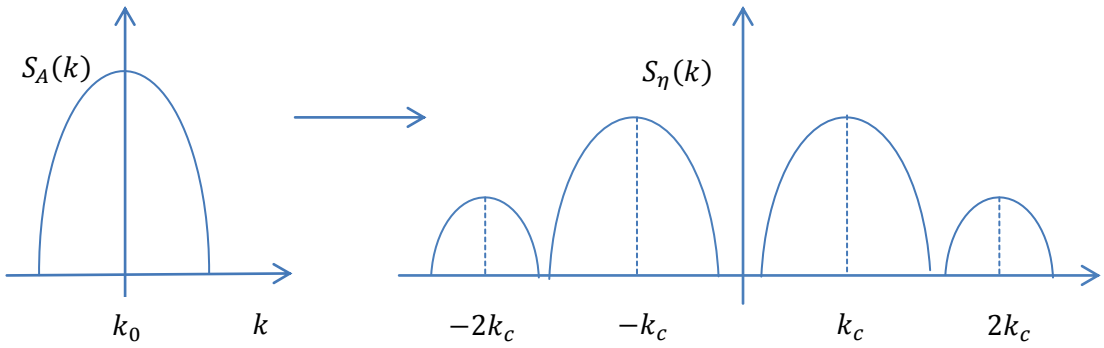

Figure 5.1: A sketch of narrow banded $S_A(k)$ and $S_\eta(k)$

A very bad situation can happen when we generate the wave spectrum (See Figure 5.2) If the bandwidth of $S_A(k)$ is wide, the two peaks of $S_\eta(k)$ will overlap with each other, which possibly creates another significant peak. Therefore we must modify the value of k_n in equation (11) so that $S_\eta(k)$ is narrow-banded and the overlapping area is not very big.

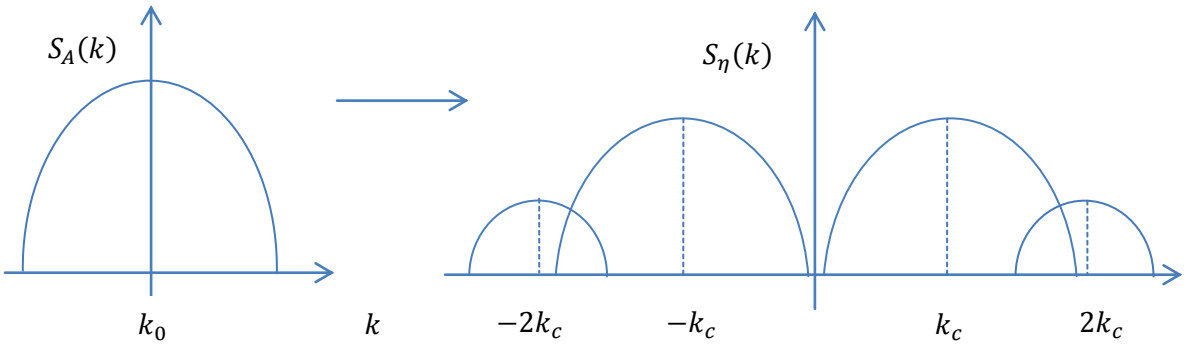

Figure 5.2: A sketch of wide banded $S_A(k)$ and $S_\eta(k)$

5.5 Initial condition setup

We shall model $S_A(k)$ with Gaussian spectrum. The benefit of choosing this spectrum is very obvious if we compare it with P&M spectrum. The wind speed U is the only input parameter in P&M spectrum, which makes it impossible to fix the spectral width, but for Gaussian spectrum, the width appears to be an input parameter-σ right away, thus easily controllable. The two dimensional Gaussian spectrum is given by:

$$S(k_x, k_y) = \frac{\varepsilon^2}{4\pi\sigma_x\sigma_y} e^{-\frac{(k_x-k_c)^2}{2\sigma_x^2}-\frac{k_y^2}{2\sigma_y^2}} \quad (13)$$

[10]

In order to get the 1D spectrum, we integrate equation (13) over k_y and get:

$$S(k_x) = \int_{-\infty}^{\infty} \frac{\varepsilon^2}{4\pi\sigma_x\sigma_y} e^{-\frac{(k_x-k_p)^2}{2\sigma_x^2}-\frac{k_y^2}{2\sigma_y^2}} d(k_y)$$

$$= \frac{\varepsilon^2}{4\pi\sigma_x\sigma_y} e^{-\frac{(k_x-k_p)^2}{2\sigma_x^2}} \int_{-\infty}^{\infty} e^{-\frac{k_y^2}{2\sigma_y^2}} d(k_y)$$

$$= \frac{\varepsilon^2}{4\pi\sigma_x} e^{-\frac{(k_x-k_p)^2}{2\sigma_x^2}} \int_{-\infty}^{\infty} e^{-\frac{\left(\frac{k_y}{\sigma_y}\right)^2}{2}} d\left(\frac{k_y}{\sigma_y}\right)$$

$$= \frac{\varepsilon^2}{4\pi\sigma_x} e^{-\frac{(k_x-k_p)^2}{2\sigma_x^2}} . (\sqrt{2\pi})$$

Then the amplitude spectrum $S_A(k)$ is:

$$S_A(k) = \frac{\varepsilon^2}{2\sqrt{2\pi}\sigma} e^{-\frac{(k-k_p)^2}{2\sigma^2}} \quad (14)$$

Where k_p, σ, ε are the peak wave number, spectral width, steepness respectively. Notice that k_p must be set to 0 in order to satisfy the criterion we discussed in the last section. To have a one-sided spectrum of $S_\eta(k)$, we apply the normalization rule and get:

$$\int_{-\infty}^{\infty} 2S_A(k)dk = R_A(0)$$

$$\int_{-\infty}^{\infty} 2S_A(k)dk = \sum_n B_n^2$$

$$B_n = \sqrt{2S_A(k_n)\Delta k}$$

To make the spectrum narrow banded we set $\sigma = 0.1$ and $k_N = k_{\max} = 2k_c$.

Matlab code for the initial input:

```
function y=initial1(x,kc)
d_k=0.0125;
k_max=2*kc;
```

```
k_min=-2*kc;
k=k_min:d_k:k_max;
J=(k_max-k_min)/d_k+1;
%Gaussian spectra.
epsillon=0.1;
sigma=0.1;
S=epsillon^2/(2*sqrt(2*pi)*sigma)*exp(-k.^2/(2*sigma^2));
B=sqrt(2*S*d_k);
%surface elevation by Gaussian spectra
A=0;
for j=1:J
    A_frag=B(j)*exp(i*(k(j)*x+2*pi*rand(1)));
    A=A+A_frag;
end
%plots
figure;plot(x,A,'b',x,-i*A,'r');
y=A;
```

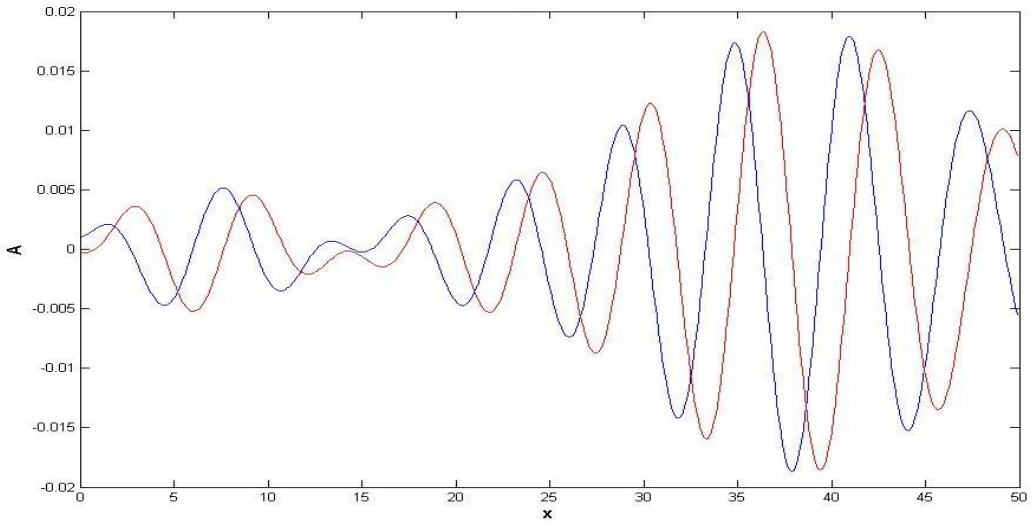

Figure 5.3: Initial amplitude $A(x, 0)$ in a zoomed distance

(real part –curve starting above 0, imaginary part –curve starting below 0)

5.6 The appearance of waves and wave spectra

In this section we shall study the phenomena of waves with respect to the steepness and the numerical experiments are done by the following characteristic groups.
Group 1: $\varepsilon = 0.01, k_c = 1, \sigma = 0.1$

Group 2: $\varepsilon = 0.1, k_c = 1, \sigma = 0.1$

Group 3: $\varepsilon = 0.5, k_c = 1, \sigma = 0.1$.

Surface elevation for group 1

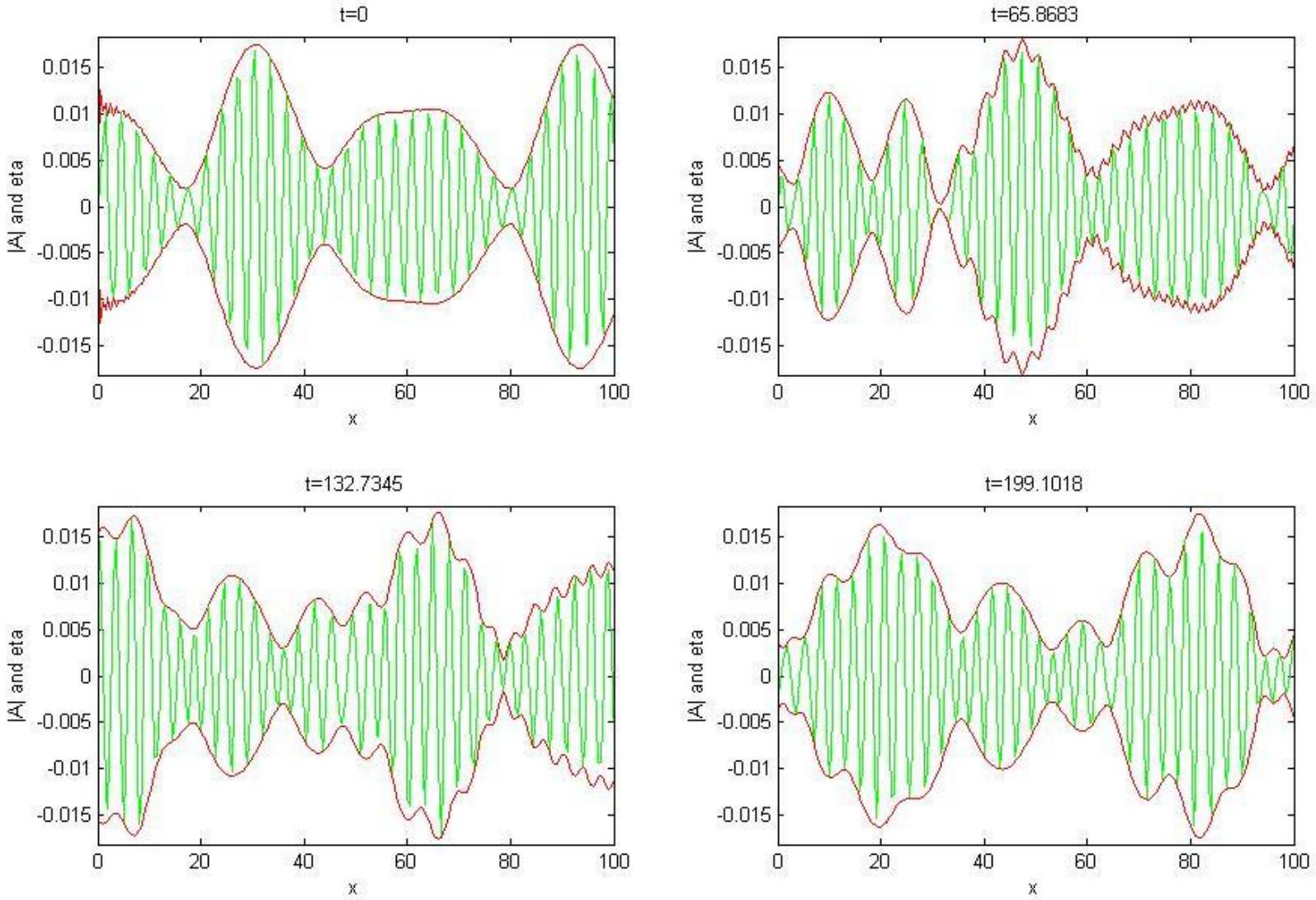

Figure 5.4 : surface elevation with $\varepsilon = 0.01, k_c = 1, \sigma = 0.1$

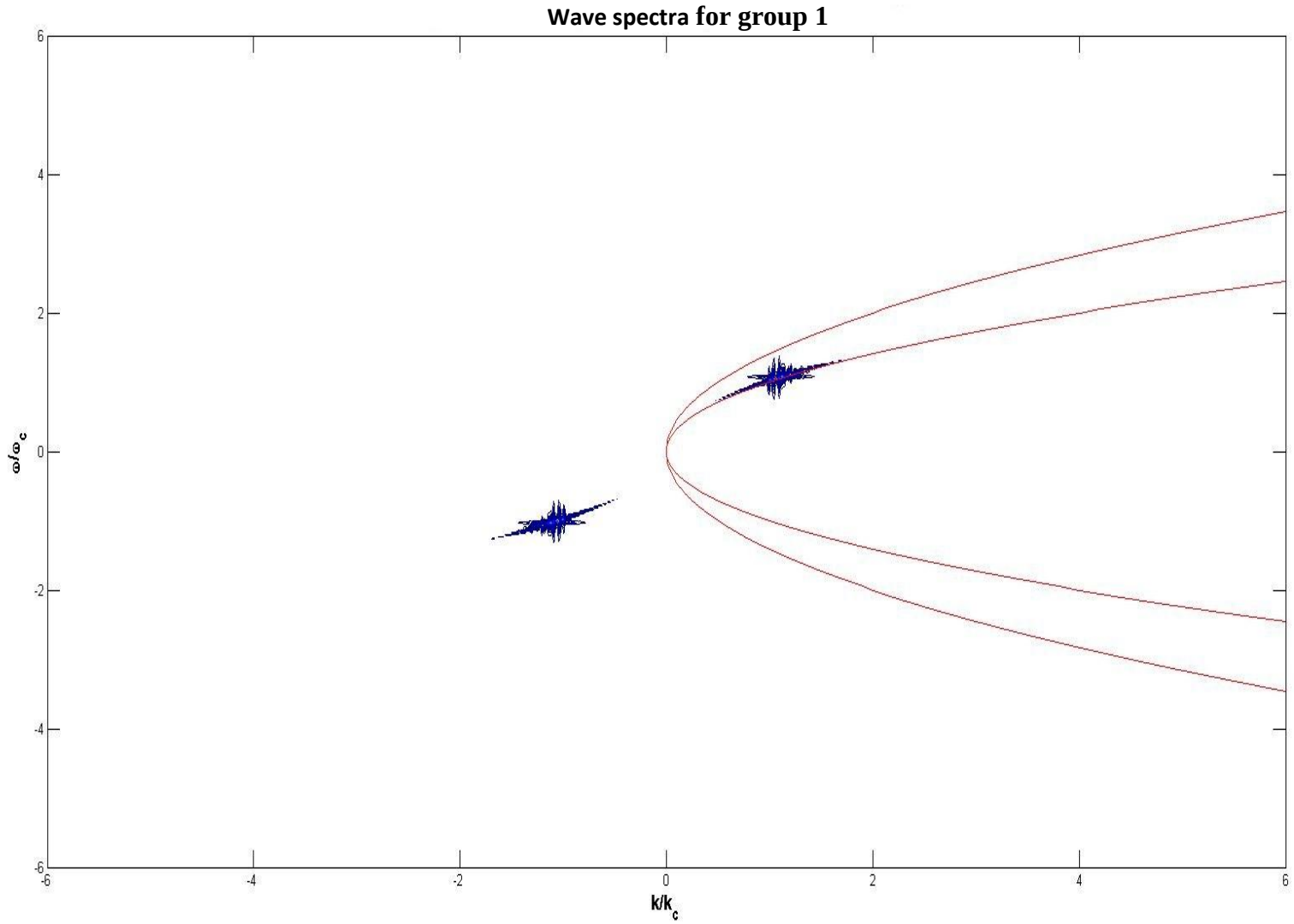

Figure 5.5: wave spectra with $\varepsilon = 0.01, k_c = 1, \sigma = 0.1$, energy on the second shell is not visible in the linear plot.

Surface elevation for group 2

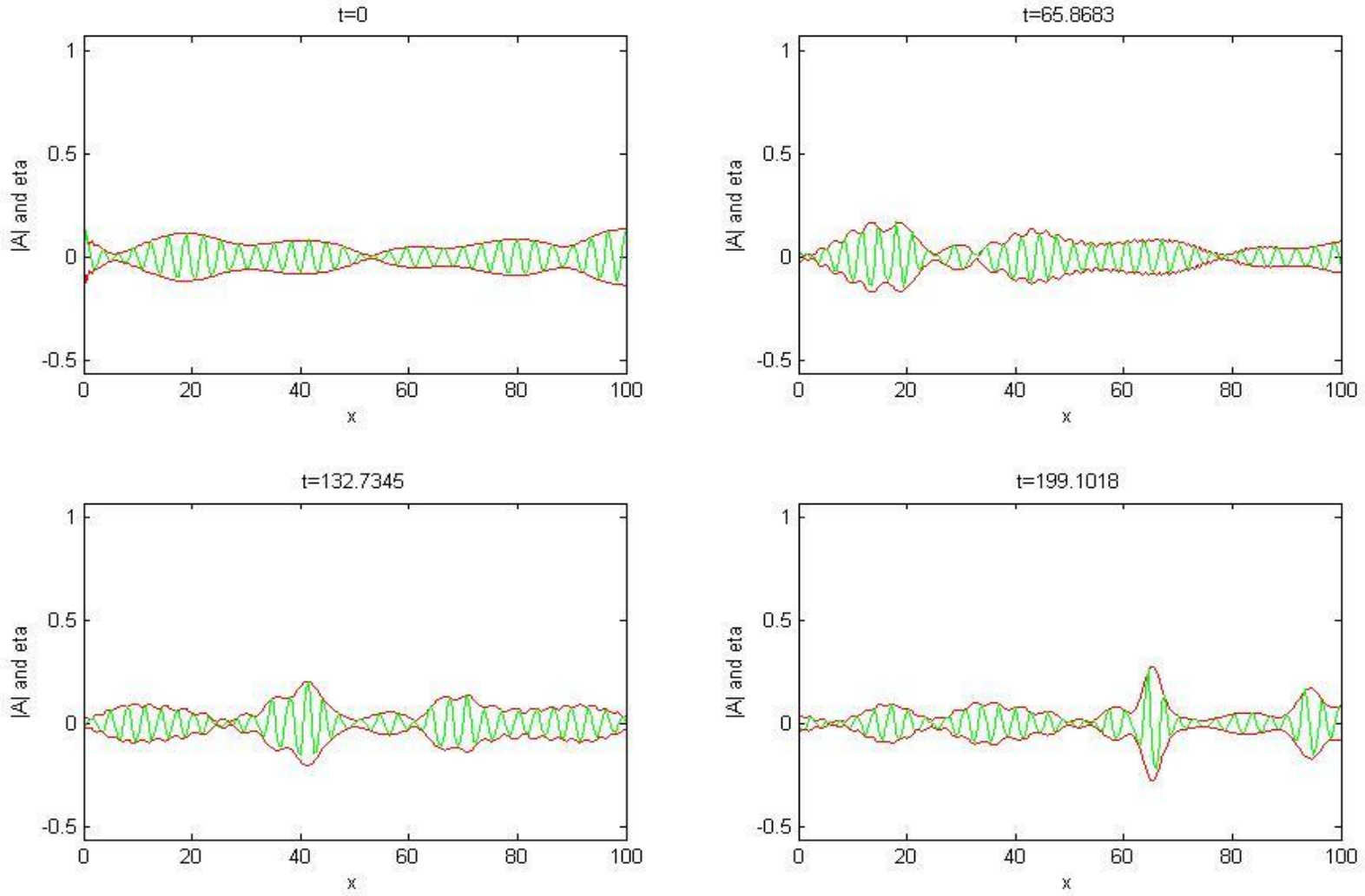

Figure 5.6: surface elevation with $\varepsilon = 0.1, k_c = 1, \sigma = 0.1$

Wave spectra for group 2

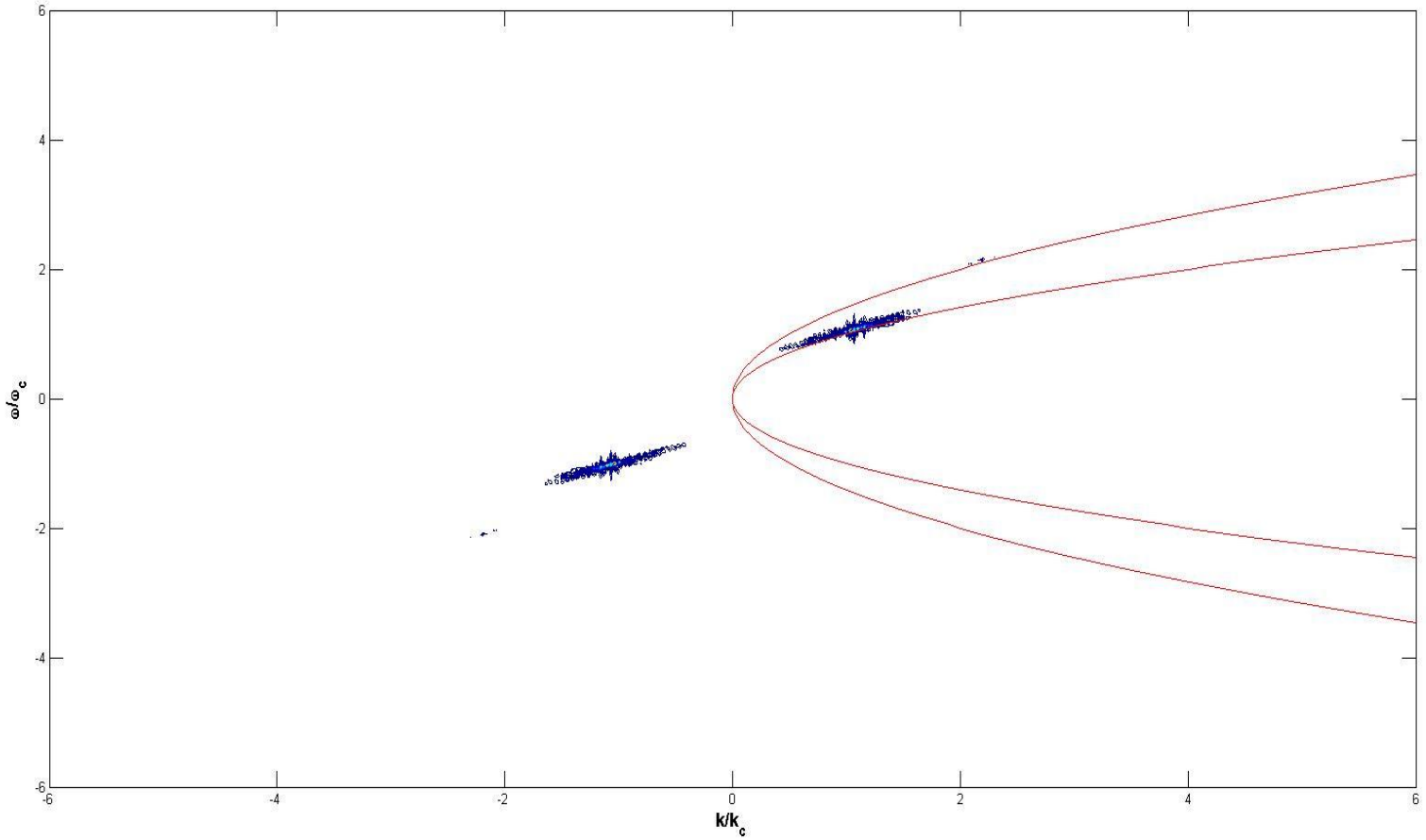

Figure 5.7: wave spectra with $\varepsilon = 0.1, k_c = 1, \sigma = 0.1$.

Surface elevation for group 3

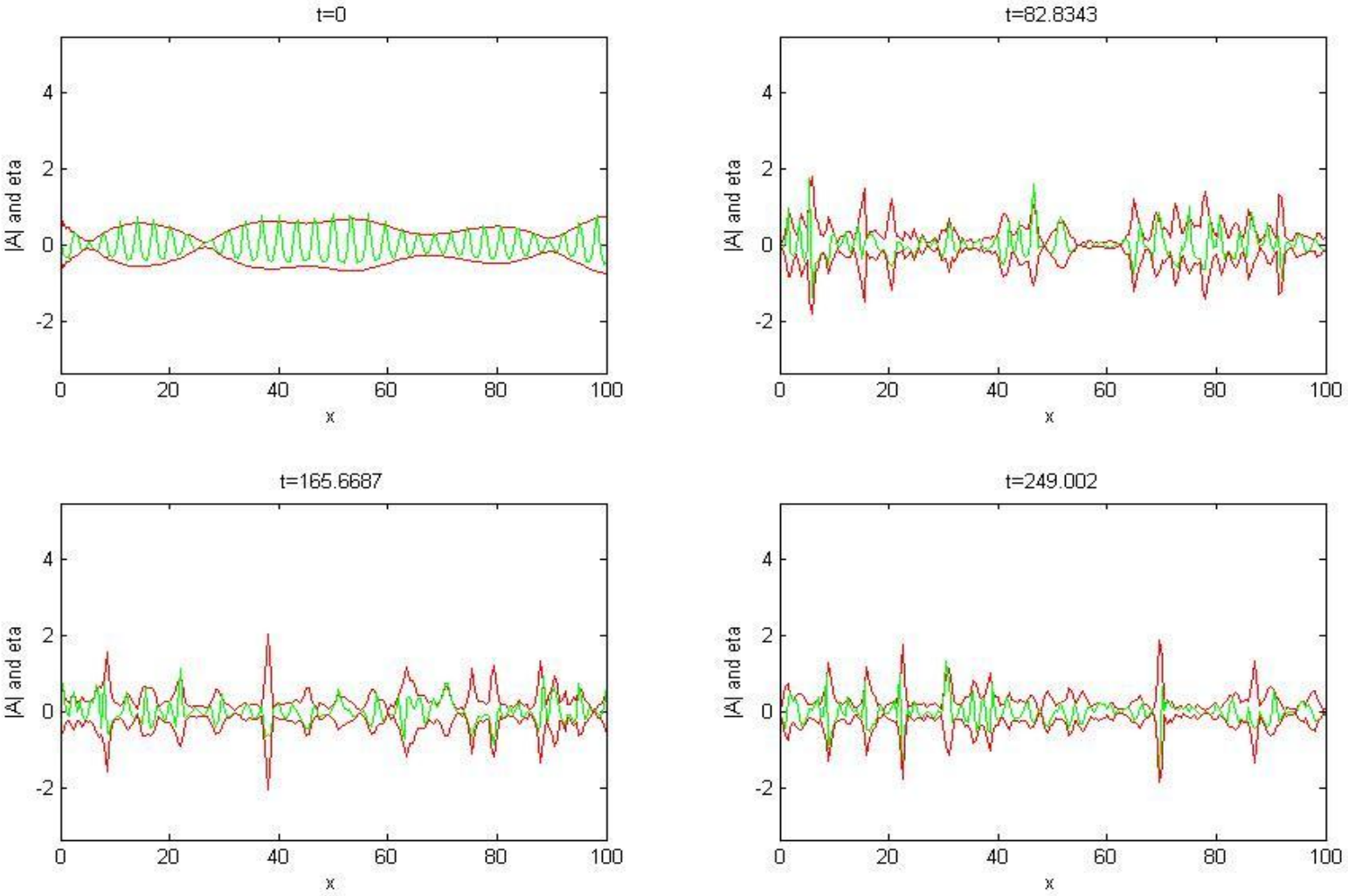

Figure 5.8: surface elevation with $\varepsilon = 0.5, k_c = 1, \sigma = 0.1$

First of all, we observe from the wave plots that $|A|$ acts as the envelope of the waves, and the waves behave nicely within it. Secondly, we observe from Figure 5.4, 5.6, 5.8 that as the steepness gets bigger, the surface elevation becomes very steep (see figure 5.8) and does not correspond to the phenomena in reality. To generate more realistic waves, a limitation of the value of the steepness should be defined, that is $\varepsilon \leq 0.1$[11]. Finally, from Figure 5.5, 5.7, we see spectra with two different shapes due to the steepness. When the steepness is small, the contours tend to follow the harmonic shells. When it is big, they appear to be tangent to the shells at point $(1,1)$.

5.7 Image spectra by Fourier analysis.

The shadow masks are found by the same numerical algorithm introduced in Chapter 2 (see Figure 5.8). As my numerical experiments showed that even if the wave spectra look very different regarding to the steepness, the image spectra of the corresponding shadow masks have almost the same appearance: there are infinitely many contours allocate tangently to the harmonic shells. (See Figure 5.9)

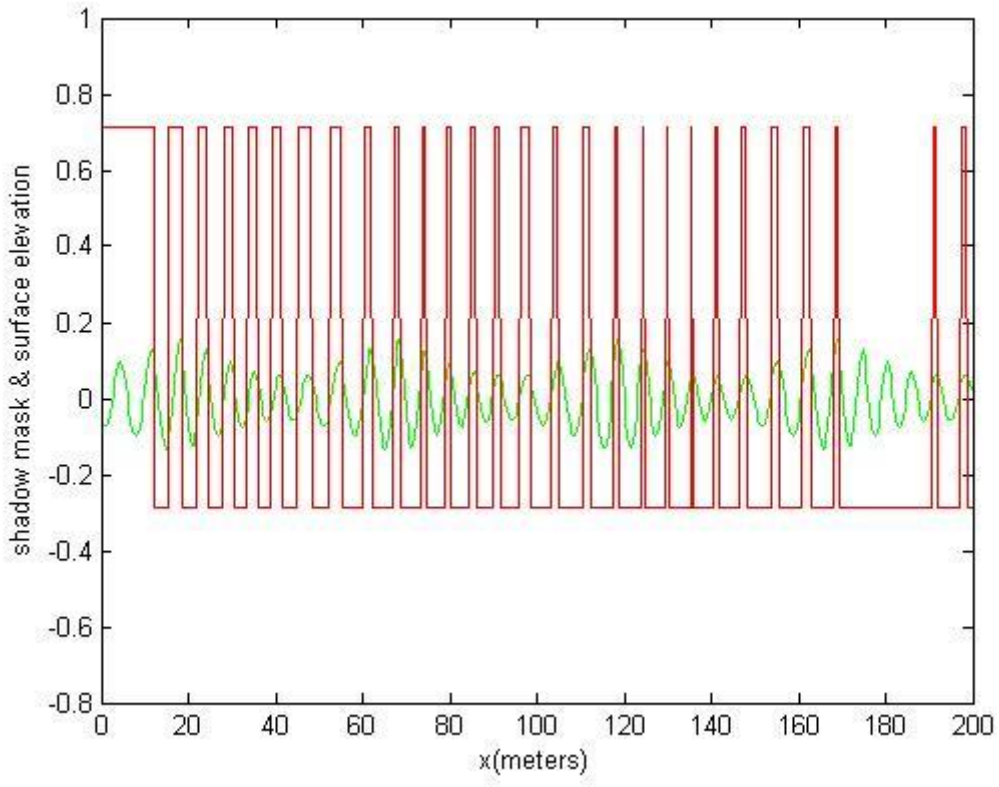

Figure 5.8: Shadow masks found by radar set to $(\mathbf{0}, \mathbf{1})$

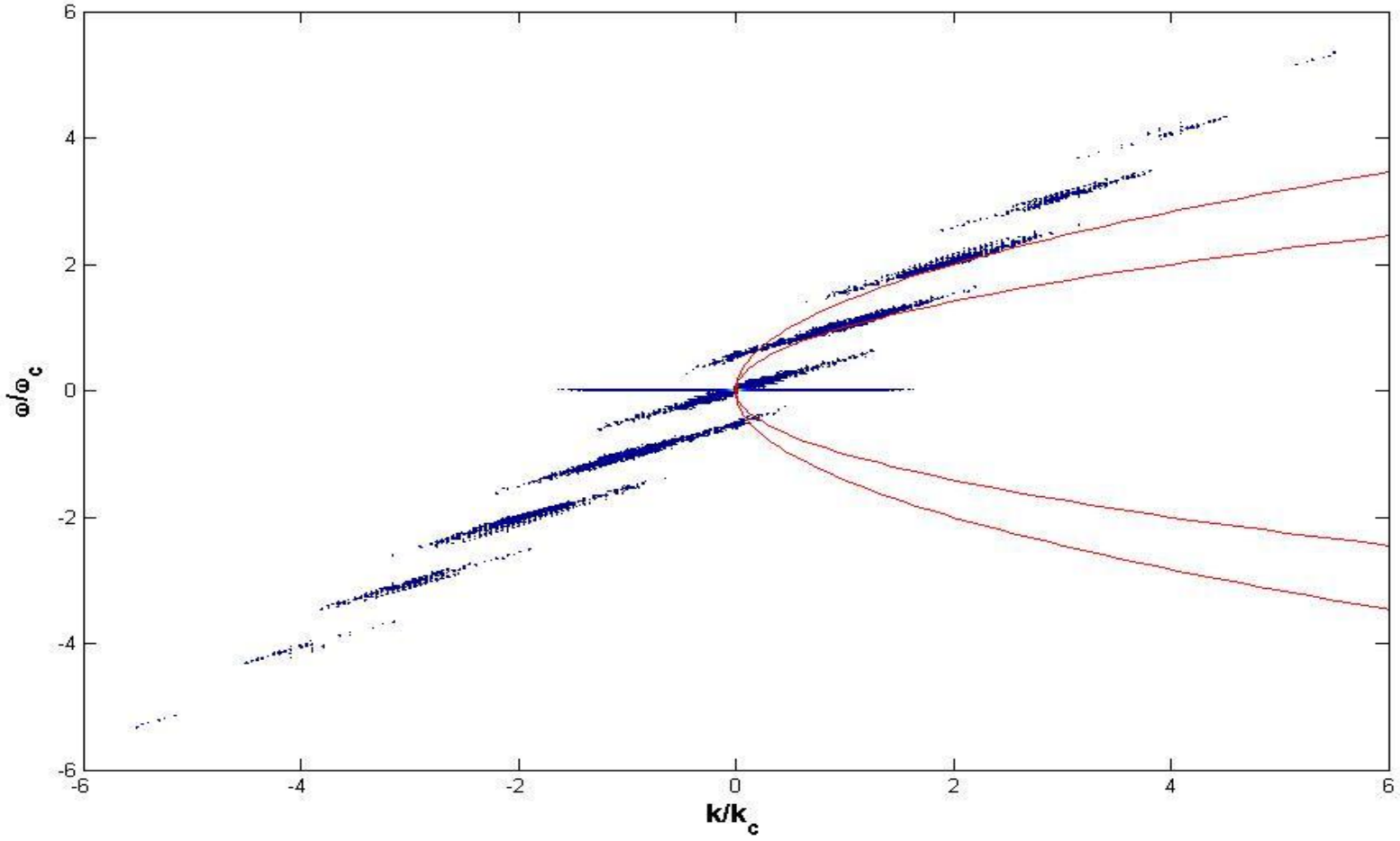

Figure 5.9: Image spectra of shadow masks with $\varepsilon = 0.1, \sigma = 0.1$

5.8 Extracting wave information from shadow masks

By comparing Figure 5.7, 5.9, we notice that the image spectra contain the information of the original waves as well as the noise caused by the nonlinearity of the shadow masks. Since the construction of the waves are of the 2nd order, wave information spreads out on the 1st and 2nd harmonic shells of the image spectra. What is the proportion of the wave information to the noise on the two shells? We shall investigate the problem by looking at the wave number spectrum of both the waves and the shadow masks.

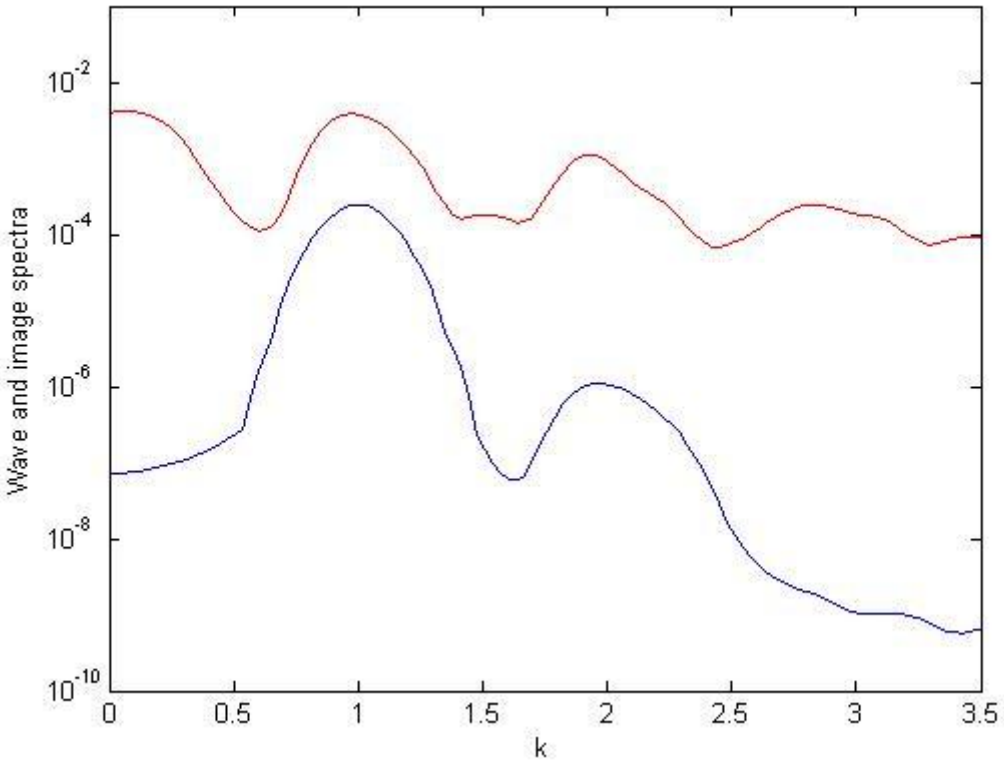

Figure 5.10: Wave number spectra of waves (lower) and shadow masks (upper), $\varepsilon = 0.1$

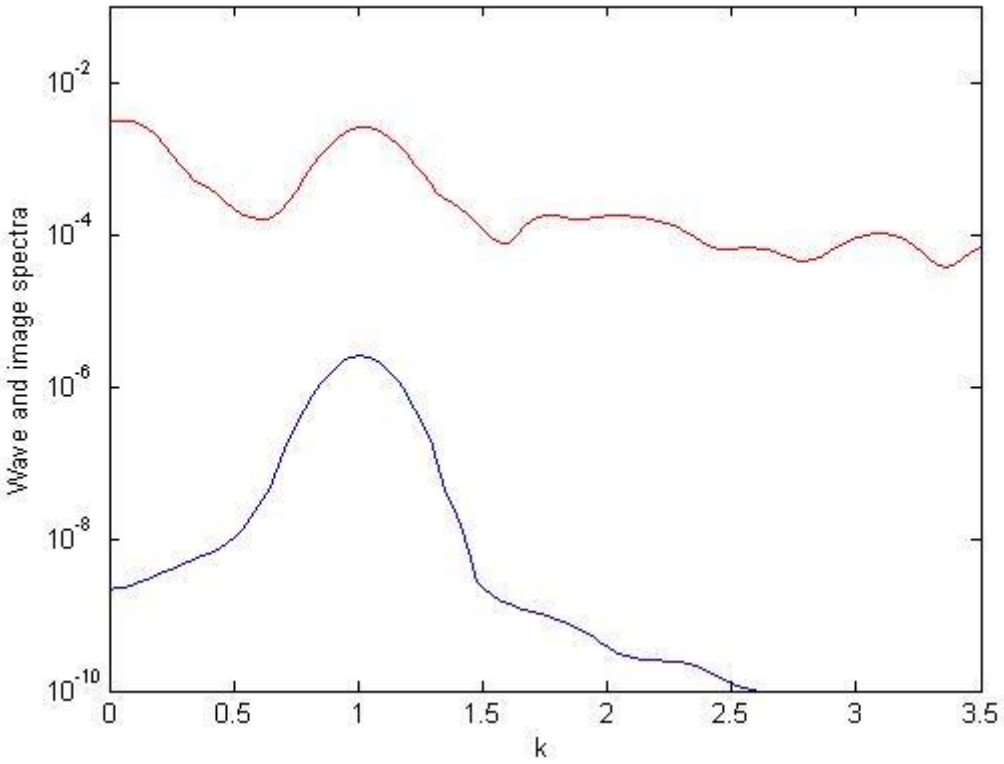

Figure 5.11: Wave number spectra of waves (lower) and shadow masks (upper), $\varepsilon = 0.01$

When the steepness is 0.1 (see Figure 5.10), the first peak of the wave spectrum (blue peak at $k = 1$) is nearly 10 times smaller in value than its corresponding peak of the image spectrum (the red peak at $k = 1$), the second peak of the wave spectrum (blue peak at $k = 2$) has an even smaller value, thus worthless to compare with the red peak above it. When the steepness is 0.01 (see Figure 5.11), the wave spectrum loses the second peak and becomes even smaller in values, while the image spectrum nearly fluctuates around the same logarithmic level. Therefore we conclude that, for both cases, the noise is more significant than the wave information on the 1st and 2nd harmonic shells.

The first term (1st order wave component) in equation (9) creates noise on all the harmonic shells and preserves its wave information to the 1st harmonic shell of the image spectrum. The second term (2nd order wave component) in equation (9) further increases the noise on all the shells and preserves its wave information to the 2nd harmonic shell of the image spectrum. We shall concentrate on the effect of how much noise is added on both the 1st and 2nd harmonic shells by the 2nd order wave component. Therefore, we need to filter out the energy on both shells of the image spectrum for both the 1st and 2nd order surface reconstructions of the waves. Since the contours look very much like straight bars, we use line-functions as their skeletons and filter out everything within a certain bandwidth around the line-functions. (See Figure 5.12, 5.13)

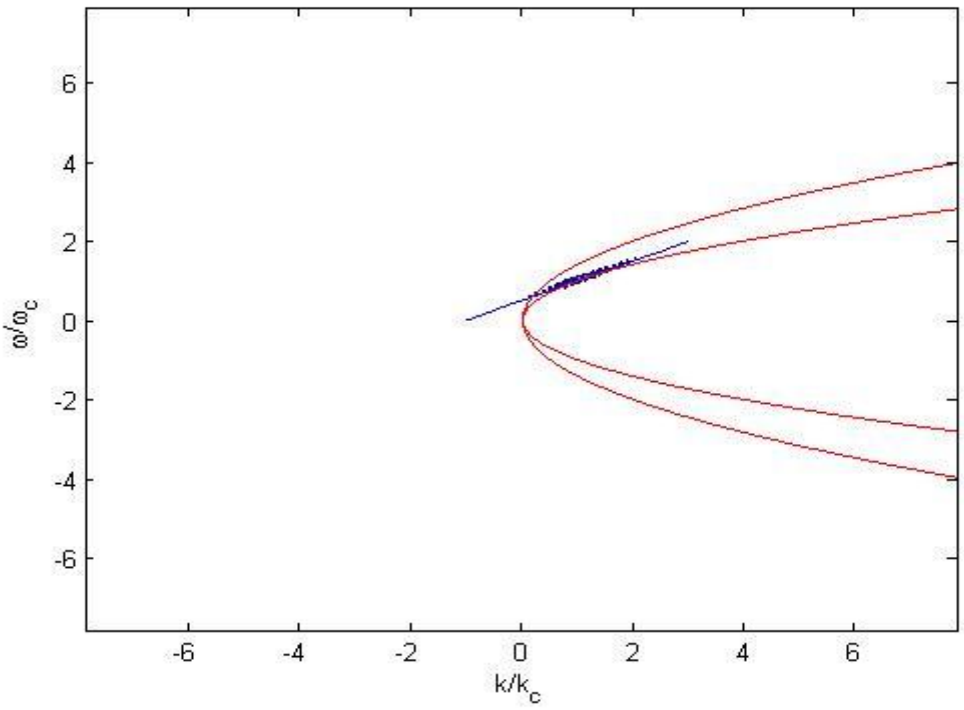

Figure 5.12: The line-function tangent to the 1st harmonic shell at point (1,1) and the contour filtered out.

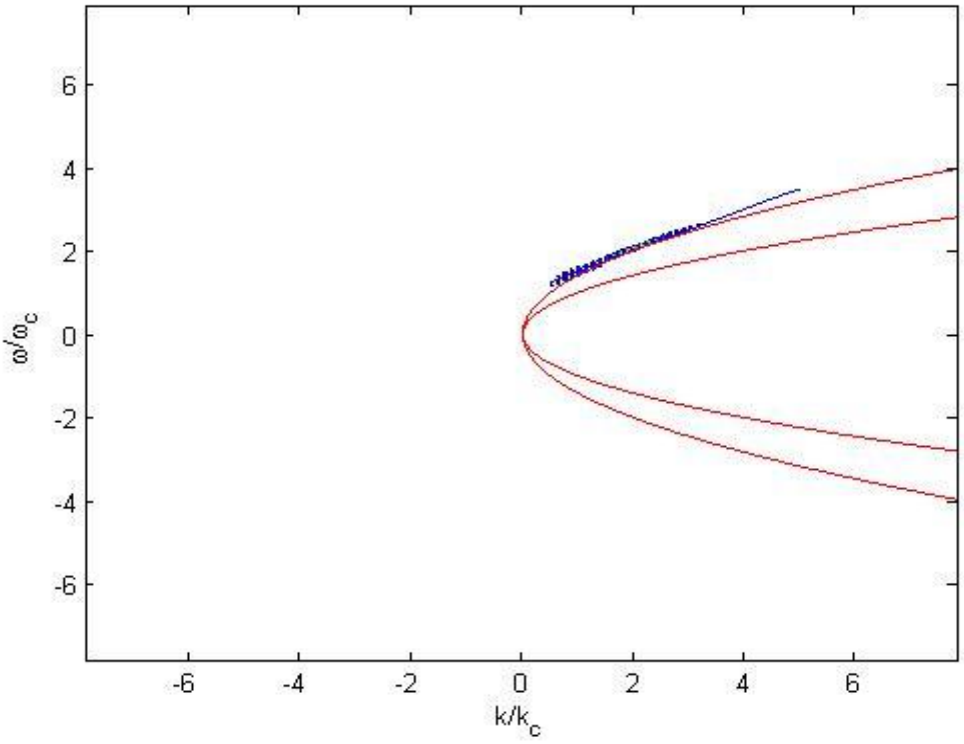

Figure 5.13: The line-function tangent to the 2nd harmonic shell at point (2,2) and the contour filtered out.

Matlab code for the filtering method:

```
function picc(data,O)
%If O=1, we filter out the energy on the 1st harmonic shell. If O=2, we do
the same for the 2nd harmonic shell.
%Get useful information from the file.
structure=load(data,'-mat');
L=structure.L;
T=structure.T;
eta=structure.eta; %eta can be waves or shadow masks.
kc=structure.kc;
omegac=sqrt(kc*9.8);
%measure the size of surface elevation matrix.
s=size(eta);
N=s(1);% num. of discrete points in t-dimonsion.
M=s(2);% num. of discrete points in x-dimonsion.
g=9.8;
%DFT for the surface elevation.
eta_hat=1/N*fft(ifft(eta).').';
eta_hat=fftshift(eta_hat);
eta_estimator=(abs(eta_hat)).^2;
%reconstruct omega for plots.
n_omega=1:N;
omega2=2*pi*(n_omega-round(N/2))/(T);
%reconstruct k for plots
n_k=1:M;
k2=2*pi*(n_k-round(M/2))/(L);
[k,omega]=meshgrid(k2,omega2);
%function tl() is the filtering method for the 1st harmonic shell.
if O==1
      [xxx,yyy,eta_filted]=tl(kc,kc,L,T,M,N,k2,omega2,eta_estimator);
End
%function tl2() is the filtering method for the 2nd harmonic shell.
if O==2
      [xxx,yyy,eta_filted]=tl2(2*kc,kc,L,T,M,N,k2,omega2,eta_estimator);
end
figure;
%plot the line-function and the filtered contour.
contour(k,omega,eta_filted,100);hold on;plot(xxx,yyy);
%plot the two harmonic shells
xx=-6*omegac:0.05*omegac:6*omegac;
yy=(xx).^2/g/kc;
plot(yy,xx/omegac,'r',yy/2,xx/omegac,'r');xlabel('k/k_c');ylabel('\omega/\o
mega_c');


function [k,omega,eta_filted]=tl(k0,kc,L,T,M,N,k2,omega2,eta)
%k0 is the tangent point (here k0=kc).
g=9.8;
omegac=sqrt(kc*g);
%find the slope (tan) of the line-function
p_index=round(k0*L/(2*pi))+round(M/2)+1
k_1=k2(p_index)/kc;
omega_1=sqrt(k2(p_index)*g)/omegac;
k_2=k2(p_index+1)/kc;
omega_2=sqrt(k2(p_index+1)*g)/omegac;
tan=(omega_2-omega_1)/(k_2-k_1);
%the length of the line-function.
k=-1:2*pi/L:3;
omega=tan*(k-k_1)+omega_1;
omega_indexs=round(omega*T/(2*pi))+round(N/2);
```

```
k_indexs=round(k*L/(2*pi))+round(M/2)+1;
J=length(omega_indexs);
for j=1:J
    omega(j)=omega2(omega_indexs(j));
end
%define the bandwidth.
omega_upper_indexs=omega_indexs+3;
omega_lower_indexs=omega_indexs-2;
%eta_filted stores the filtered energy.
eta_filted=zeros(N,M);
l=0;
for i=k_indexs(1):k_indexs(J)
    l=l+1;
    for j=omega_lower_indexs(l):omega_upper_indexs(l)
        eta_filted(j,i)=2*eta(j,i);
    end
end


function [k,omega,eta_filted]=tl2(k0,kc,L,T,M,N,k2,omega2,eta)
%k0 is the tangent point (here k0=2*kc).
g=9.8;
omegac=sqrt(kc*g);
%find the slope (tan) of the line-function
p_index=round(k0*L/(2*pi))+round(M/2)+1
k_1=k2(p_index)/kc
omega_1=sqrt(2*k2(p_index)*g)/omegac
k_2=k2(p_index+1)/kc
omega_2=sqrt(2*k2(p_index+1)*g)/omegac
tan=(omega_2-omega_1)/(k_2-k_1)
%the length of the line-function.
k=0.5:2*pi/L:5;
omega=tan*(k-k_1)+omega_1;
%find the indexes of omega and k
omega_indexs=round(omega*T/(2*pi))+round(N/2);
k_indexs=round(k*L/(2*pi))+round(M/2)+1;
J=length(omega_indexs);
for j=1:J
    omega(j)=omega2(omega_indexs(j));
end
%define the bandwidth.
omega_upper_indexs=omega_indexs+3;
omega_lower_indexs=omega_indexs-2;
eta_filted=zeros(N,M);
l=0;
for i=k_indexs(1):k_indexs(J)
    l=l+1;
    for j=omega_lower_indexs(l):omega_upper_indexs(l)
        eta_filted(j,i)=2*eta(j,i);
    end
end
```

We shall carry out numerical experiments with the above code and collect data. Before that we shall define some key words for the convenience of writing. We shall call the image spectra of the shadow masks generated by the 1st order waves "the 1st order image spectra" and the image spectra of the shadow masks generated by the 2nd order waves "The 2nd order image spectra". The input parameters are set to: $H_r(\text{radar height}) = 1(\text{meter})$, $L = 200(\text{meters})$, $T = 200(\text{seconds})$,$M = 500$,$N = 500$,$k_c = 1$,$\varepsilon = 0.1$,$\sigma = 0.1$. By changing the phase shifts ϕ_j-s for each group, we have the follow statistics for the energy distribution.

		Group1	Group2	Group3	Group4
1st order wave spectra	1st harmonic	0.0047	0.0049	0.0047	0.0048
	2nd harmonic	-	-	-	-
2nd order wave spectra	1st harmonic	0.0047	0.0049	0.0047	0.0048
	2nd harmonic	0.00006	0.00002	0.000062	0.000044
1st order image spectra	1st harmonic	0.0692	0.075	0.0667	0.0778
	2nd harmonic	0.0179	0.0239	0.0171	0.0227
2nd order image spectra	1st harmonic	0.0616	0.068	0.0594	0.0703
	2nd harmonic	0.0171	0.0228	0.0162	0.0217

Table 5.14: Energy distribution on the 1st and 2nd harmonic shells for both wave and image spectra

We observe from Table 5.14 that the energy on the 2nd harmonic shell of the wave spectra is very tiny comparing to that on the 1st harmonic shell of the same spectra. By adding this tiny energy, the 1st order wave spectra become the 2nd order wave spectra, and the 1st order image spectra become the 2nd order image spectra. Since the filtering method also takes some unwanted noise into account, the statistics may have some round-off errors. But in a certain degree, the differences between the values in the last and third-last row can describe how much wave information is added on the 2nd harmonic shell. We conclude that the addition is very tiny and thus the wave information is much less than the noise on this shell. When the steepness of the waves are even smaller than 0.1, we can deduct that the 2nd order wave component is worthless to consider.

Chapter 7 Conclusion

This thesis is a combination of mathematical formulations and numerical implementations. The derivation of the mathematical models uses the knowledge in mathematics, mechanics and statistics while the numerical algorithms contain some personal ideas.

In this thesis, I have generated the wave and image spectra based on the synthetic wave fields and extracted the wave information from shadow masks with special attention to the second harmonic shell. My numerical results showed that: For the second order nonlinear waves generated by the NLS equation, the wave information on the second harmonic shell is too tiny to consider comparing to the noise on the same shell. This is probably due to the limitation of the steepness($\varepsilon < 0.1$), which upper bounds the wave amplitudes to around 0.1 meter. For the second order waves generated by the nonlinear extension of linear wave theory, the wave information on the second harmonic shell becomes more and more considerable as the wave height increases. It seems that the wave information on the second harmonic shell depends on the actual wave height. If the actual wave height on the ocean surface is very big, the signal-to-noise ratio in the empirical formula would not be correct, which leads to an incorrect estimation of the actual significant wave height. If the actual wave height on the ocean surface is small, the wave information on the second harmonic shell is neglectable and the empirical formula would be fine.

Bibliography

[1]. Trulsen K, Weakly nonlinear and stochastic properties of ocean wave fields: Application to an extreme wave event, Mechanics Division, Department of Mathematics, University of Oslo, Norway.

[2]. http://www.codecogs.com/code/engineering/fluid_mechanics/waves/spectra/pierson_moskowitz.php.

[3]. http://en.wikipedia.org/wiki/Discrete_Fourier_transform.

[4]. Juglard HS, Dysthe K, Trulsen K, Krogstad HE, Liu JD, Probability distributions of surface gravity waves during spectral changes, J. Fluid Mech.(2005) 542: 195-216.

[5]. Buckley JR, Can Geometric Optics Fully Describe Radar Images of the Sea Surface at Grazing Incidence, Geoscience and Remote Sensing Symposium (2001) 4: 1732-1734.

[6]. Seemann J, Ziemer F, Senet CM, A Method for Computing Calibrated Ocean Wave Spectra from Measurements with a Nautical X-Band Radar, OCEANS (1997) 2: 1148-1154.

[7]. Lo E, Mei CC, A numerical study of water-wave modulation based on a higher-order nonlinear Schrödinger equation, J. Fluid Mech. (1985) 150: 395-416.

[8]. http://en.wikipedia.org/wiki/Split-step_method.

[9]. Thiab R. Taha, M J. Ablowitz, Analytical and Numerical Aspects of Certain Nonlinear Evolution Equations. II. Numerical, Nonlinear Schrodinger Equation, Journal of Computational Physics (1984) 55:211-212.

[10]. Gramstad O, Trulsen K, Influence of crests and group length on the occurrence of freak waves, J. Fluid Mech. (2007) 582: 463-472.

[11]. Krogstad HE, Trulsen K, Interpretations and observations of ocean wave spectra, Ocean Dynamics (2010) 60: 973-991.